A Density Functional Theory Study on the Effect of Ge Alloying on Hydrogen Desorption from SiGe Alloy Surfaces

Collin Mui[†] **and Stacey F. Bent**

Department of Chemical Engineering, Stanford University, Stanford California 94305

Charles B. Musgrave*

Departments of Chemical Engineering and Materials Science and Engineering, Stanford University, Stanford California 94305

Received: December 19, 2003; In Final Form: February 25, 2004

We have used density functional theory to investigate hydrogen desorption from SiGe alloy surfaces, and the effect of Ge alloying on the kinetics of hydrogen desorption via the prepairing and interdimer mechanisms. We find that the calculated activation barriers of the prepairing mechanism are affected by the surface atom bonded to the desorbing hydrogen atoms. On the other hand, our calculations show that the activation barrier for hydrogen desorption via the 2H interdimer mechanism is affected by all four surface atoms of the two neighboring dimers. For the 4H interdimer mechanism, we have shown that the activation barrier for hydrogen desorption is not significantly higher than the endothermicity of hydrogen desorption. We also find that the calculated activation barriers of the interdimer mechanisms are generally lower than those of the prepairing mechanism. In addition, our calculations show that surface Ge atoms on neighboring dimers on SiGe alloy surfaces have a minor effect on the calculated activation barriers of both the prepairing and interdimer mechanisms, which indicates that the effect of Ge alloying on hydrogen desorption is local in nature. We also discuss the effects of cluster size and constraints on the calculated reaction energies and activation barriers of hydrogen desorption via the two mechanisms.

I. Introduction

Silicon−germanium (SiGe) alloy thin films are of growing importance in modern high performance field-effect transistors (FET) and bipolar junction transistors (BJT) for high-speed complementary metal-semiconductor-oxide (CMOS) circuits and wireless telecommunication systems.[1,2] In addition, SiGe alloys enable optoelectronic and quantum-effect device technologies in Si-based systems.[3,4] Therefore, there has been a significant interest in the deposition of SiGe alloy thin films in recent years.

Deposition of SiGe alloys is commonly achieved by chemical vapor deposition (CVD) or gas-source molecular beam epitaxy (GSMBE) with Si and Ge hydrides as gas-phase precursors.[5−7] It is well-known that the presence of GeH_4 in a SiGe deposition source gas mixture enhances the growth rate of SiGe alloys compared to epitaxial Si growth, and the effect has been attributed to the enhanced hydrogen desorption rate when Ge is present on the surface during growth.[8−11] However, the mechanism by which Ge alloying affects hydrogen desorption chemistry is still unclear. Therefore, attempts to predict SiGe deposition have previously relied on phenomenological surface chemistry models with experimentally determined kinetic parameters interpolated from the pure components.[12−16]

The effect of Ge on hydrogen desorption has motivated a number of experimental studies on both Ge-covered Si(100)[17−21] and SiGe alloy surfaces,[22−24] resulting in two proposed explanations for the effect of Ge on hydrogen desorption kinetics. The "long-range-electronic-effect model" attributes the decrease in activation barriers to electronic effects of Ge atoms on the surface, which weaken the Si−H bonds and thus decrease the activation barrier of hydrogen desorption.[17,23,24] The "Ge−H intermediate model" assumes the activation barriers for hydrogen desorption from Si sites and Ge sites are independent of the surface Ge concentration and describes the desorption process in terms of migration of hydrogen from Si to Ge sites, followed by rapid desorption of H_2 from the Ge sites.[18−22]

The surface chemistry of hydrogen on semiconductors is closely coupled to surface reconstruction. The (100) face of group-IV semiconductor surfaces undergoes a dimer reconstruction, in which adjacent surface atoms pair up and form dimer rows to minimize the surface energy.[25] The (100) surface of SiGe alloys also undergoes reconstruction, leading to Si−Si, Ge−Ge, and Ge−Si dimers, each of which has been observed on Ge/Si(100) and SiGe/Si(100) surfaces experimentally.[26−32] Scanning tunneling microscopy (STM) studies provide direct evidence for the existence of dimer row domains on both Ge/Si(100) and SiGe/Si(100) surfaces.[33−37]

According to temperature programmed desorption (TPD) experiments, the position of the desorption peak temperature of H_2 from the monohydride phase of the Si(100)-2×1 surface does not vary with initial hydrogen coverage. This indicates that hydrogen desorption follows first-order kinetics. Since the initial observation of near-first-order desorption of hydrogen from the Si(100)-2×1 surface,[38] there have been numerous experimental and theoretical investigations on the mechanism and associated kinetics of hydrogen desorption from group-IV semiconductor surfaces.[38−61] Several mechanisms have been

* Corresponding author. E-mail: chasm@stanford.edu.
[†] Present address: Novellus Systems, Inc., 4000 North First Street, San Jose, CA 95134.

10.1021/jp037948a CCC: $27.50
Published on Web 04/27/2004

SCHEME 1

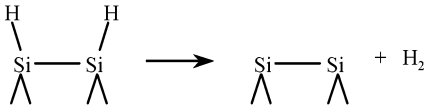

SCHEME 2

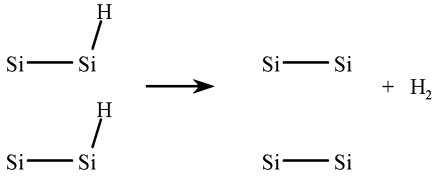

proposed on the basis of these experiments, including the prepairing,[38,41,42,49] dihydride,[47,48,51,52] and interdimer mechanisms,[55,59,60] as well as desorption via an excited electronic state.[58] This paper focuses on the reaction energies and activation barriers of hydrogen desorption via the prepairing and interdimer mechanisms because these two mechanisms are fundamentally distinctive, in that they involve a different number of surface sites. Therefore, it is likely that surface Ge atoms on SiGe alloy surfaces have characteristic but unique effects on the energetics of hydrogen desorption via each of these two mechanisms.

In the prepairing mechanism, shown in Scheme 1, two hydrogen atoms pair up on a surface dimer and recombine to form H_2 which desorbs directly from the dimer. The prepairing mechanism involves only one surface dimer and is a natural consequence of the weak $\pi-$interaction between the two atoms of a bare dimer, which results in a thermodynamic driving force for surface hydrogen atoms to pair up on a single dimer of (100) semiconductor surfaces. The prepairing mechanism has been incorporated into a lattice gas model to explain the near-first-order kinetics of hydrogen desorption from the Si(100)-2×1 and Ge(100)-2×1 surfaces.[42,44,62,63]

Despite its simplicity, the prepairing mechanism is the focus of many theoretical studies. Although calculations employing cluster models for the surface tend to overestimate the activation barrier for hydrogen desorption from the Si(100)-2×1 surface compared to the values derived from temperature programmed desorption (TPD) experiments,[45−49,51] recent density functional theory (DFT) calculations suggest that the discrepancies may originate from the inadequate cluster size used in the calculations.[57,61] In particular, calculations employing larger clusters for the Si(100)-2×1 surface result in lower activation barriers for hydrogen desorption via the prepairing mechanism.[57,61]

Recent scanning tunneling microscopy (STM) and second harmonic generation (SHG) studies suggest an alternative model in which hydrogen adsorption and desorption occur via interdimer mechanisms from the Si(100)-2×1 surface.[55,59,60] Interdimer mechanisms involve recombinative desorption from two Si−H bonds on two adjacent dimers along a dimer row. Three interdimer mechanisms have been proposed on the basis of STM and SHG experiments.[55] In the 2H desorption mechanism shown in Scheme 2, hydrogen atoms recombinatively desorb from two adjacent singly occupied dimers. The 3H mechanism in Scheme 3 involves desorption from adjacent singly and doubly occupied dimers. Finally, the 4H desorption mechanism in Scheme 4 involves desorption from adjacent doubly occupied dimers.

SHG experiments have indicated that the adsorption probability of H_2 onto the Si(100)-2×1 surface via interdimer mechanisms follows the order 4H > 3H > 2H, and the measured adsorption probabilities are consistent with DFT-calculated activation barriers for adsorption.[60] In addition, a model based

SCHEME 3

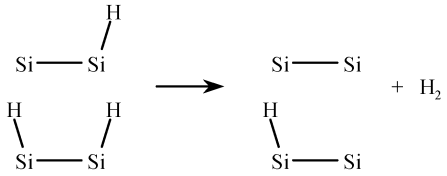

SCHEME 4

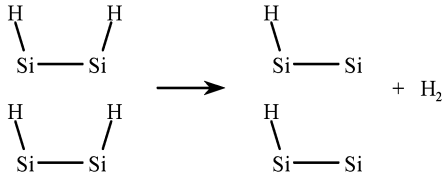

on microscopic reversibility and statistical mechanics has been applied to explain hydrogen adsorption and desorption on the Si(100)-2×1 surface via interdimer mechanisms,[59] and the fitted kinetic parameters are consistent with DFT calculations.[60] The statistical mechanics model also predicts that the 4H desorption pathway dominates at high hydrogen coverage, whereas the 2H pathway becomes important at low coverages.[59]

This paper presents a detailed DFT study of hydrogen desorption from SiGe alloy surfaces via prepairing and interdimer mechanisms. A combined quantum chemical and statistical model for the simulation of temperature programmed desorption of hydrogen from SiGe alloy surfaces is presented in a separate publication.[64] Because there are relatively fewer studies on SiGe alloy surfaces despite the extensive theoretical and experimental studies that have been performed on the Si(100)-2×1 surface, we focus on the effect of Ge alloying atoms on the kinetics of hydrogen desorption. We have calculated the energies and activation barriers of hydrogen desorption via both the prepairing and the interdimer mechanisms using cluster models to represent SiGe alloy surfaces. In addition, we have also investigated the effects of cluster size and constraints on the calculated reaction energies and activation barriers.

II. Computational Details

A. Cluster Models for SiGe Alloy Surfaces. We model the Si(100)-2×1 surface using clusters of silicon atoms. The Si_9H_{12} one-dimer cluster consists of two surface and seven subsurface Si atoms (Figure 1a). The truncated bulk Si−Si bonds are terminated with Si−H bonds using twelve hydrogen atoms to preserve the sp^3 hybridization of the subsurface Si atoms. The Si_9H_{12} one-dimer cluster mimics the main characteristics of a Si−Si dimer on the Si(100)-2×1 surface, including the weak $\pi-$bond of the dimer. To model SiGe alloy surfaces, $Ge_2Si_7H_{12}$ and $GeSi_8H_{12}$ one-dimer clusters are used (Figure 1b−d). The $Ge_2Si_7H_{12}$ cluster contains a Ge−Ge homodimer and seven subsurface Si atoms, whereas the $GeSi_8H_{12}$ cluster contains a Ge−Si heterodimer on the surface. These clusters are designed to study the effect of surface Ge atoms on the chemistry of SiGe alloy surfaces.[65] Our DFT calculations show that the one-dimer clusters are tilted, especially for the Ge-containing clusters. The effect of bulk Ge atoms on the chemistry of SiGe alloy surfaces is studied by replacing the subsurface Si atoms in the $Ge_2Si_7H_{12}$ cluster with Ge atoms, resulting in the Ge_9H_{12} one-dimer cluster (Figure 1e).

Hydrogen desorption via the interdimer mechanism is studied using two-dimer clusters. The $Si_{15}H_{16}$ cluster consists of two adjacent dimers along a dimer row (Figure 2a). Similar to the one-dimer clusters, the truncated Si−Si bulk bonds are termi-

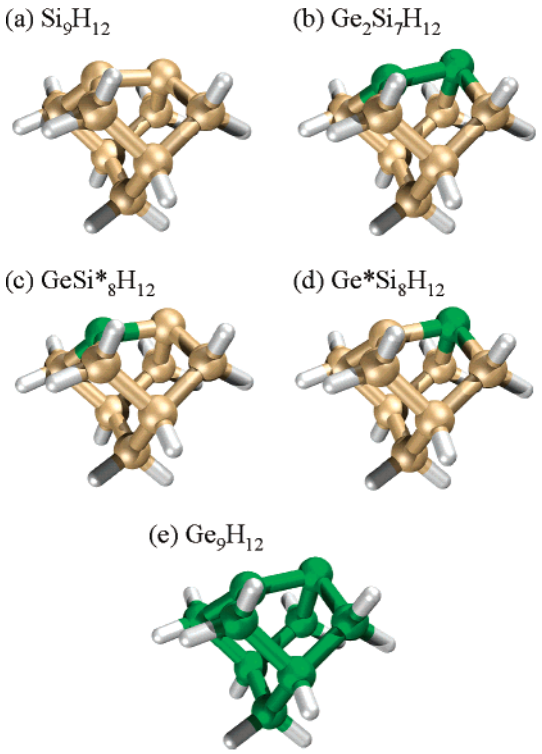

Figure 1. One-dimer clusters used in the calculations: (a) Si_9H_{12}; (b) $Ge_2Si_7H_{12}$; (c) $GeSi^*_8H_{12}$; (d) $Ge^*Si_8H_{12}$; (e) Ge_9H_{12}. The asterisks denote the "up" atom.

nated with hydrogen atoms. To study the effect of surface Ge on hydrogen desorption via the interdimer mechanism, the $Ge_2Si_{13}H_{16}$ and $Ge_4Si_{11}H_{16}$ two-dimer clusters were used to model SiGe alloy surfaces. The $Ge_4Si_{11}H_{16}$ cluster consists of two Ge−Ge homodimers on the surface (Figure 2b). Three $Ge_2Si_{13}H_{16}$ two-dimer clusters were considered: the homo-$Ge_2Si_{13}H_{16}$ cluster consists of a Si−Si and a Ge−Ge homodimer (Figure 2c), the adj-$Ge_2Si_{13}H_{16}$ cluster consists of two Ge−Si heterodimers in which the two Ge atoms are adjacent to each other along the dimer row (Figure 2d), and the alt-$Ge_2Si_{13}H_{16}$ cluster consists of two Ge−Si heterodimers in which the two Ge atoms are on opposite sides of the dimer row (Figure 2e,f).

To investigate the effect of neighboring dimers on hydrogen desorption from SiGe alloy surfaces via the prepairing mechanism, several three-dimer clusters are also employed. The $Si_{21}H_{20}$ cluster consists of three adjacent dimers with six surface Si atoms along a dimer row. SiGe alloy surfaces are modeled by several three-dimer clusters, in which the surface Si dimer atoms are replaced by Ge atoms. The $Ge_2Si_{19}H_{20}$ and $GeSi_{20}H_{20}$ three-dimer clusters are obtained by replacing the central dimer of the $Si_{21}H_{20}$ cluster with a Ge−Ge homodimer and a Ge−Si heterodimer, respectively. The $Ge_6Si_{15}H_{20}$ cluster, which consists of three Ge−Ge homodimers on the surface, is designed to investigate the effect of neighboring Ge dimer atoms on the chemistry of SiGe alloy surfaces.

Four-dimer clusters are used to investigate cluster size effects on the calculated energetics for the interdimer mechanisms. In particular, the $Si_{27}H_{24}$ cluster consists of four adjacent dimers with eight Si atoms. Four-dimer clusters mimicking SiGe alloy surfaces are obtained by replacing surface Si atoms with Ge. For example, the $Ge_4Si_{23}H_{24}$ cluster consists of two Ge−Ge dimers occupying the two dimer sites on the center of the cluster and two Si−Si dimers on the two edge sites. Similarly, the $Ge_8Si_{19}H_{24}$ cluster consists of 4 Ge−Ge homodimers on the surface of the cluster.

B. Theoretical Approach. Our theoretical approach is based on DFT[66,67] employing the B3LYP three-parameter hybrid exchange-correlation functional[68] as implemented in the Gaussian 98 computational chemistry software package.[69] The electronic structure is expanded in a mixed Gaussian basis set. In the mixed basis set scheme, a triple-ζ plus polarization and diffuse functions 6-311++G(d,p) basis set is used for the active surface Si, Ge, and H atoms. A double-ζ plus polarization 6-31G(d) basis set is used for all subsurface Si and Ge atoms as well as terminating hydrogen atoms. The mixed basis scheme is applied to enhance the accuracy for bonds involving the chemically active atoms while minimizing the overall computational time. Important minima and transition states are verified to have zero and one imaginary frequency, respectively. In frequency calculations of structures optimized without geometric constraints, terminating hydrogen atoms are assigned masses identical to silicon (28 amu), to mimic the Si atoms in the bulk, and to decouple their motion from the surface Si−H bonds. Zero-point energies for the prepairing and interdimer mechanisms are determined from calculations on one- and two-dimer clusters, respectively. We find that the difference between the

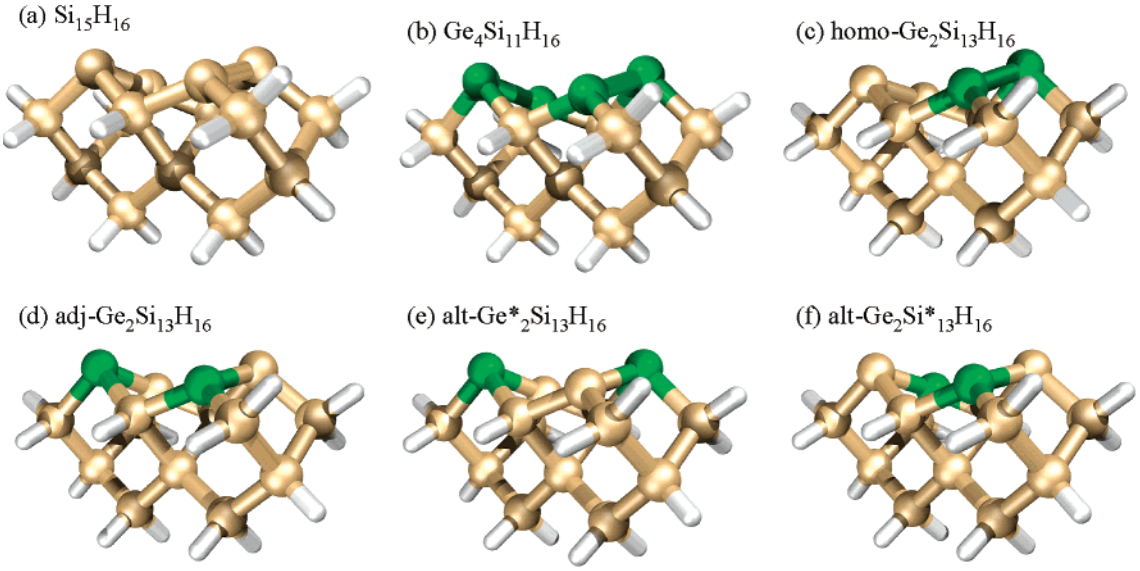

Figure 2. Two-dimer clusters: (a) $Si_{15}H_{16}$; (b) $Ge_4Si_{11}H_{16}$; (c) homo-$Ge_2Si_{13}H_{16}$; (d) adj-$Ge_2Si_{13}H_{16}$; (e) alt-$Ge^*_2Si_{13}H_{16}$; (f) alt-$Ge_2Si^*_{13}H_{16}$. The asterisks denote the "up" atom.

zero-point energies calculated with clusters terminated with "silicon-like" hydrogen atoms (28 amu) and those calculated with clusters terminated with "normal" hydrogen atoms (1 amu) is less than 0.2 kcal/mol.

C. Geometry Optimizations. Geometry optimizations are performed both with and without geometric constraints, and symmetry restrictions are applied where appropriate. The constrained clusters are constructed using a two-step procedure to create boundary conditions on the terminating hydrogens as follows. In the first step of the constrained optimization procedure, the lowest layer Si atom is fixed in space. The third layer Si atoms are constrained according to their positions relative to the lowest layer Si atom in the perfect crystal and are only allowed to move normal to the surface. The four second layer Si atoms are allowed to freely relax within a symmetry plane containing the lowest layer Si atom and perpendicular to the direction of the dimer row. The top layer Si dimer atoms are completely unconstrained.

The positions of the terminating hydrogens are also constrained by fixing the Si−H bonds along the directions of the Si−Si bonds they represent. The hydrogens terminating the bottom layer Si atom are fixed in tetrahedral directions with a Si−H bond length of 1.495 Å. The hydrogens terminating the third layer Si atoms are completely relaxed within the plane containing the three bottommost Si atoms. The terminating hydrogens representing trench Si atoms are allowed to freely relax on a plane containing the second layer Si atoms to which they are bonded and perpendicular to the direction of the dimer row. The hydrogen atoms representing neighboring Si dimer atoms are constrained to lie along the direction of the Si−Si bonds they represent. The positions of the terminating hydrogens are then determined by optimizing all unconstrained parameters, including the Si−H distances.

In the second step of the constrained optimization procedure, the terminating hydrogen atoms are fixed in space at the positions determined from the first step, and all Si and surface hydrogen atoms are allowed to fully relax. The same "hydrogen shell" is used in the calculations of the bare surface dimers, transition states, and reaction products. Constrained optimizations of SiGe alloy one-dimer clusters are performed using the same "hydrogen shell" obtained using the Si_9H_{12} one-dimer cluster to mimic the strain environment of SiGe alloy surfaces.

Constrained optimizations of two-, three-, and four-dimer clusters are performed using a similar procedure described above for the one-dimer clusters, with additional constraints imposed on the subsurface Si atoms not terminated by hydrogen atoms. The lowest layer Si atoms are fixed at crystallographic positions. The third layer Si atoms not bonded to terminating hydrogen atoms are allowed to relax within a plane containing the lowest layer Si atoms. The second layer Si atoms are allowed to freely relax within a symmetry plane perpendicular to the direction of the dimer row. The central Si−Si dimer bonds in the three- and four-dimer cluster are not allowed to rotate about the surface normal, although the dimer atoms are otherwise unconstrained.

III. Results and Discussion

A. Hydrogen Desorption via the Prepairing Mechanism. *1. Energies of Hydrogen Desorption from SiGe Alloy Dimers.* We have calculated the energies of recombinative hydrogen desorption from the monohydride phase of SiGe alloy dimers via the prepairing mechanism, where the desorption energy is defined as the energy of the bare cluster and molecular hydrogen relative to the hydrogen-terminated cluster. The optimized monohydride structures and the desorption energies on unconstrained one-dimer clusters are shown in Figure 3a−c. We find that the desorption reactions are endothermic and that the energy decreases as Si dimer atoms are replaced by Ge. This trend is consistent with the fact that the Ge−H bond is weaker than the Si−H bond, which results in lower desorption energies from Ge-containing dimers.

SCHEME 5

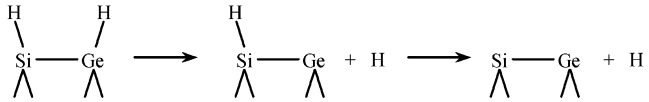

TABLE 1: Surface Si−H and Ge−H Bond Energies (kcal/mol) of Doubly and Singly Occupied Dimers[a]

bond energy	Si−Si/Ge−Ge	Ge−Si/Si−Ge
Si−H on doubly occupied dimer	80.0	80.0
Si−H on singly occupied dimer	73.7	73.8
Ge−H on doubly occupied dimer	73.8	73.9
Ge−H on singly occupied dimer	67.8	67.7

[a] The energies are calculated using one-dimer clusters and are zero-point corrected.

We have also calculated the bond energies of surface hydrogens on SiGe dimers, according to Scheme 5 above and the results are shown in Table 1. Whereas a dangling bond is formed when the first H atom is detached from the doubly occupied dimer, the dimer π−bond is formed when the second H atom is removed. Therefore, on a homodimer, the bond energy of an H atom on the doubly occupied dimer is larger than the bond energy of an H atom on the singly occupied dimer. Our calculations also show that the bond energy of an adsorbed H atom is influenced only by the surface atom to which it is bonded (Table 1). For example, the Si−H bond energy of a doubly occupied Si−Si homodimer is 80.0 kcal/mol, which is identical to the Si−H bond energy of a doubly occupied Si−Ge heterodimer. The similarity applies to both Si−H and Ge−H bond energies on either singly or doubly occupied dimers. This shows that neighboring Ge atoms have no effect on Si−H bond energies and vice versa, consistent with previous calculations.[70]

2. Activation Barriers of Hydrogen Desorption from SiGe Alloy Dimers. We first consider the prepairing mechanism on SiGe alloy surfaces, to gain some insight into the effect of Ge alloying on the kinetics of hydrogen desorption via the prepairing mechanism. The highest occupied molecular orbitals (HOMO) of the transition state structures and the calculated activation barrier, defined as the energy of the transition state for hydrogen desorption relative to the monohydride-terminated cluster, on unconstrained one-dimer clusters are shown in Figure 4. All transition state structures involve tilting of the dimers, with the two hydrogen atoms positioned above the down dimer atom. For the homodimers, there is only one unique activation barrier for hydrogen desorption via the prepairing mechanism. On the other hand, there are two possible pathways for hydrogen desorption from the Ge−Si heterodimer, namely, the Ge−Si* and Ge*−Si pathways, where the asterisk denotes the up atom of the transition state structure. For the Ge−Si* pathway, the two hydrogen atoms pair above the down Ge atom. Alternatively, for the Ge*−Si pathway, the hydrogens are positioned above the down Si atom.

The activation barriers for hydrogen desorption from the Si−Si, Ge*−Si, Si*−Ge, and Ge−Ge dimers show only two distinct values, ∼74 and ∼64 kcal/mol, for the case of one-dimer clusters. Interestingly, the calculated desorption barrier depends only on the identity of the up atom of the transition state, and not on whether the down atom of the dimer is a Si or

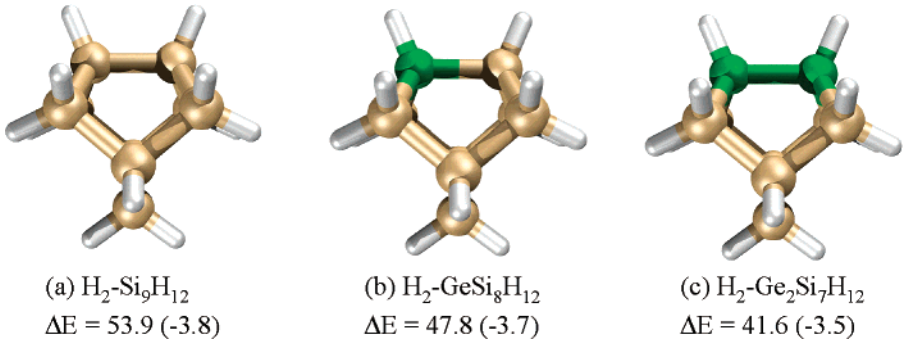

Figure 3. Monohydride structures on unconstrained SiGe one-dimers clusters: (a) $H_2-Si_9H_{12}$ one-dimer cluster; (b) $H_2-GeSi_8H_{12}$ one-dimer cluster; (c) $H_2-Ge_2Si_7H_{12}$ one-dimer cluster. Energies of hydrogen desorption are shown in kcal/mol, and the numbers in parentheses are zero-point corrections.

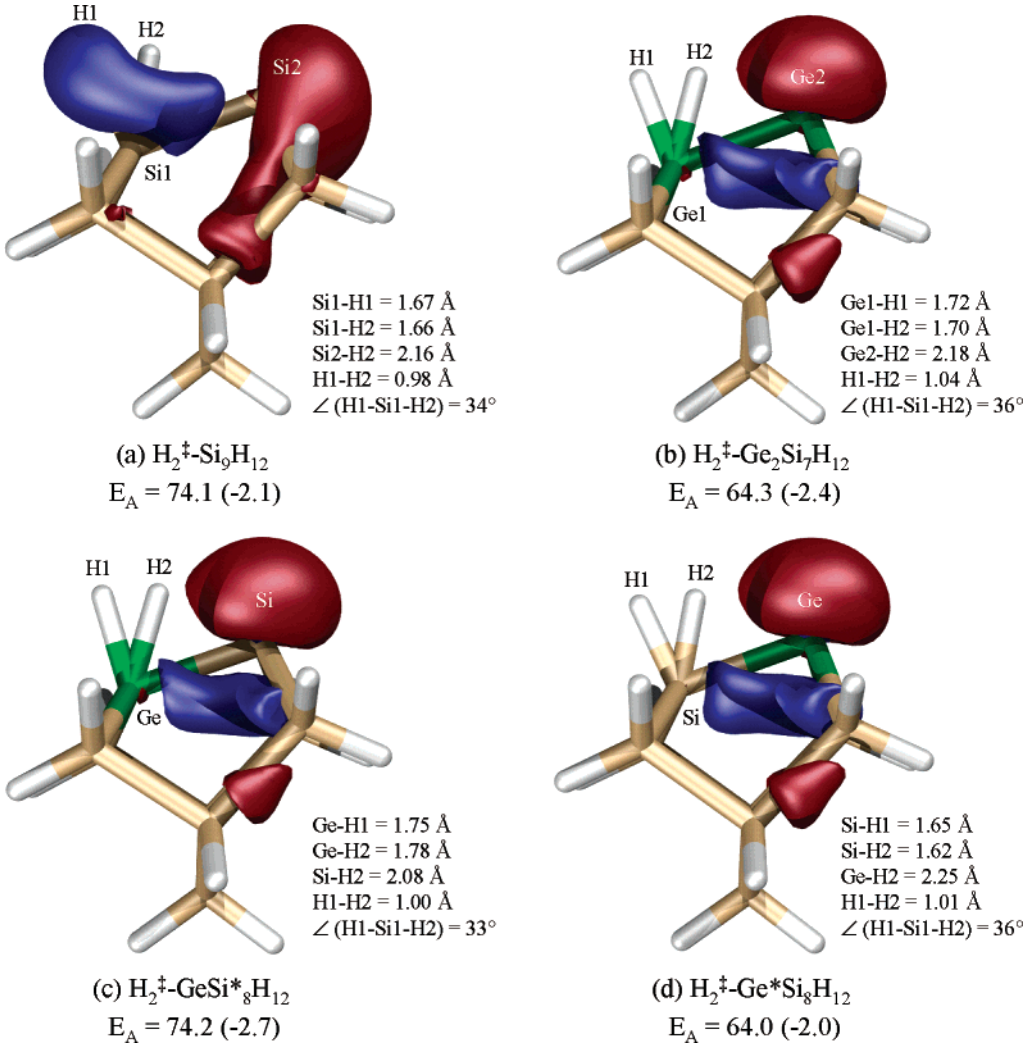

Figure 4. Transition state structures and highest occupied molecular orbitals (HOMOs) for hydrogen desorption from SiGe dimers via the prepairing mechanism: (a) $H_2^{\ddagger}-Si_9H_{12}$; (b) $H_2^{\ddagger}-Ge_2Si_7H_{12}$; (c) $H_2^{\ddagger}-GeSi^*_8H_{12}$; (d) $H_2^{\ddagger}-Ge^*Si_8H_{12}$. Activation barriers are shown in kcal/mol, and the numbers in parentheses are zero-point corrections.

Ge atom. This observation can be understood from the geometries of the transition state structures (Figure 4). We illustrate this fact using the two transition states on the Ge−Si heterodimer. Inspection of the transition state structures of the Ge−Si* and Ge*−Si heterodimers shows that most of the strain at the transition state originates from the highly stretched Si−H and Ge−H bonds to the up atom, respectively. At the Ge−Si* transition state (Figure 4c), the Si−H bond length is 2.08 Å and is 40% longer than the Si−H bond of the monohydride structure, whereas the Ge−H bond length is only 1.75 Å and is 14% longer than the surface Ge−H bond. Because the Si−H bond is stretched more than the Ge−H bond at the transition state, most of the activation energy is used to break the stronger Si−H bond, resulting in the desorption pathway with a higher activation barrier. On the other hand, the Si−H and Ge−H bond lengths are 1.65 and 2.25 Å, respectively, in the Ge*−Si transition state (Figure 4d), which are 11% and 46% longer compared to the corresponding Si−H and Ge−H bonds of the doubly occupied Ge−Si heterodimer. As a consequence, most of the activation barrier is used to break the weaker Ge−H bond,

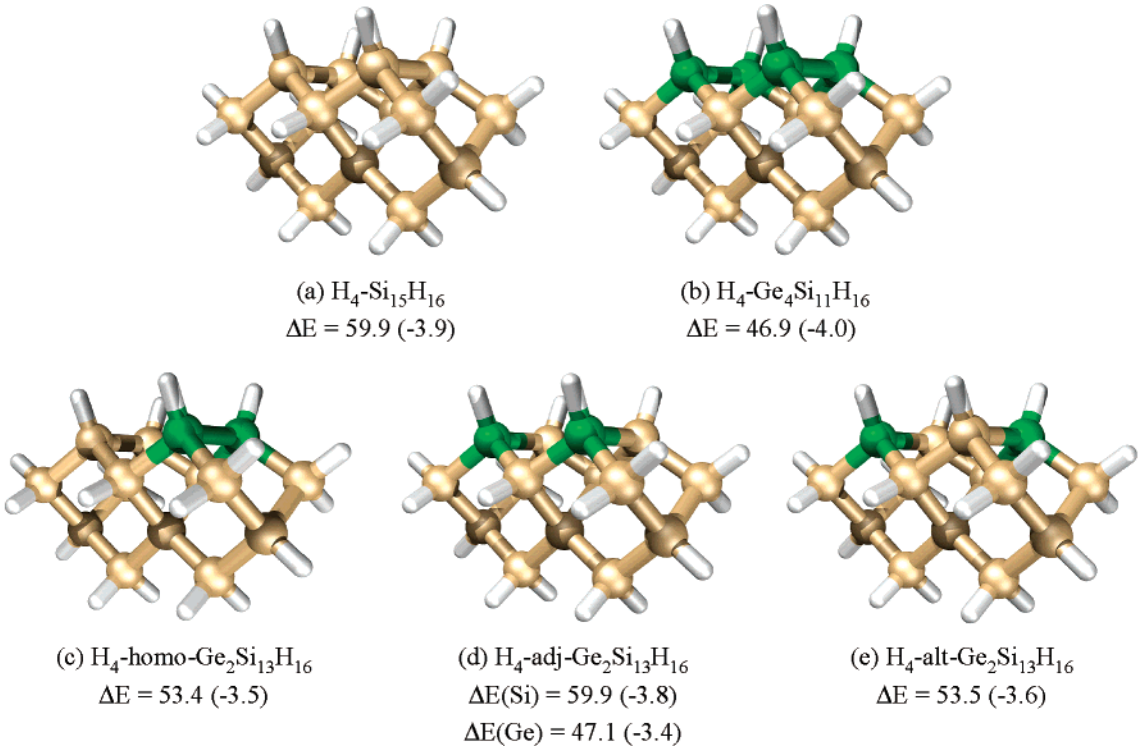

Figure 5. Optimized structures of two-dimer clusters with four adsorbed hydrogen atoms: (a) $H_4-Si_{15}H_{16}$; (b) $H_4-Ge_4Si_{11}H_{16}$; (c) homo-$H_4-Ge_2Si_{13}H_{16}$; (d) adj-$H_4-Ge_2Si_{13}H_{16}$; (e) alt-$H_4-Ge_2Si_{13}H_{16}$. Reaction energies of desorption are in kcal/mol, and the numbers in parentheses are zero-point corrections.

which results in a lower activation barrier than the Ge*−Si pathway. The transition state structures on the Si−Si and Ge−Ge homodimers also show that most of the strain at the transition states originates from the highly stretched Si−H and Ge−H bonds to the up atom, respectively. Therefore, for the cases of hydrogen desorption from the Si−Si homodimer and the Ge−Si* heterodimer, where the up atom is a Si atom, the activation barriers are ∼74 kcal/mol in both cases. On the other hand, when the up atom is Ge, as in the cases of the Ge−Ge homodimer and the Ge*−Si heterodimer, the activation barrier is lowered to ∼64 kcal/mol. Similar transition state strain arguments can be applied to explain the calculated activation barriers on the constrained one-dimer and three-dimer clusters.

B. Hydrogen Desorption via Interdimer Mechanisms. *1. Energies of Hydrogen Desorption from Adjacent Dimers.* Optimized structures and reaction energies for hydrogen desorption via the 4H, 3H and 2H interdimer mechanisms on unconstrained two-dimer clusters are shown in Figures 5−7. The calculations show that for the 4H mechanism the desorption energies are dominated by the local Si−H or Ge−H bond strengths. For example, the 4H desorption energy on the $H_4-alt-Ge_2Si_{13}H_{16}$ and $H_4-homo-Ge_2Si_{13}H_{16}$ clusters are 53.5 and 53.4 kcal/mol respectively, which are essentially identical. The same energetic trend is observed for 4H interdimer desorption from two adjacent Si atoms or two adjacent Ge atoms (Figure 5).

We find that the reaction energy for 2H desorption is mainly affected by the surface atoms to which the desorbing hydrogen atoms are bonded (Figure 7). For instance, 2H desorption from the $H_2-alt-Ge_2Si_{13}H_{16}$ and $H_2-homo-Ge_2Si_{13}H_{16}$ clusters are 38.4 and 39.5 kcal/mol, respectively. The difference of 1.1 kcal/mol between the two 2H desorption energies is only slight and originates from the two different dimer π−bonds formed from 2H desorption, because two Ge−Si heterodimer π-bonds are formed after 2H desorption from the $H_2-alt-Ge_2Si_{13}H_{16}$ surface site, whereas a Si−Si and a Ge−Ge π−bond are formed after desorption from the $H_2-homo-Ge_2Si_{13}H_{16}$ surface site.

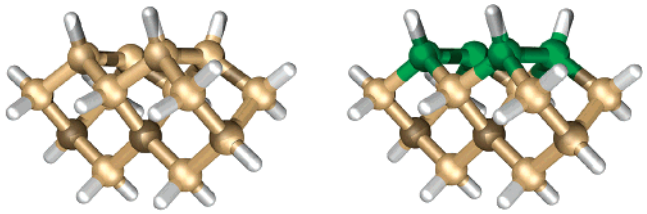

Figure 6. Optimized structures of two-dimer clusters with three adsorbed hydrogen atoms: (a) $H_3-Si_{15}H_{16}$; (b) $H_3-Ge_4Si_{11}H_{16}$.

When the energies of desorption via the three interdimer mechanisms are compared, we find that the desorption energies follow the order 4H > 3H > 2H. For instance, the desorption energies via 4H, 3H, and 2H interdimer mechanisms from the unconstrained $Si_{15}H_{16}$ two-dimer cluster are 59.9, 53.8, and 47.8 kcal/mol, respectively (Figures 5−7). Similarly, the 4H, 3H, and 2H desorption energies on the unconstrained $Ge_4Si_{11}H_{16}$ two-dimer cluster are 46.9, 40.1, and 31.4 kcal/mol (Figures 5−7). In addition, we find that the hydrogen desorption energies via the prepairing mechanism are similar to the 3H desoprtion energies. For instance, the reaction energies for hydrogen desorption via the prepairing mechanism from the Si_9H_{12} and $Ge_2Si_7H_{12}$ one-dimer clusters are 53.9 and 41.6 kcal/mol, respectively, which are very similar to the corresponding 3H desorption reaction energies on $Si_{15}H_{16}$ and $Ge_4Si_{11}H_{16}$ clusters. These energetic trends can be explained by the π-bond formation processes involved in the hydrogen desorption reaction. The 4H, 3H, and 2H desorption processes involve formation of zero, one, and two π-bonds, respectively, and hydrogen desorption via the prepairing mechanism results in the formation of one dimer π-bond. Therefore the interdimer desorption energies

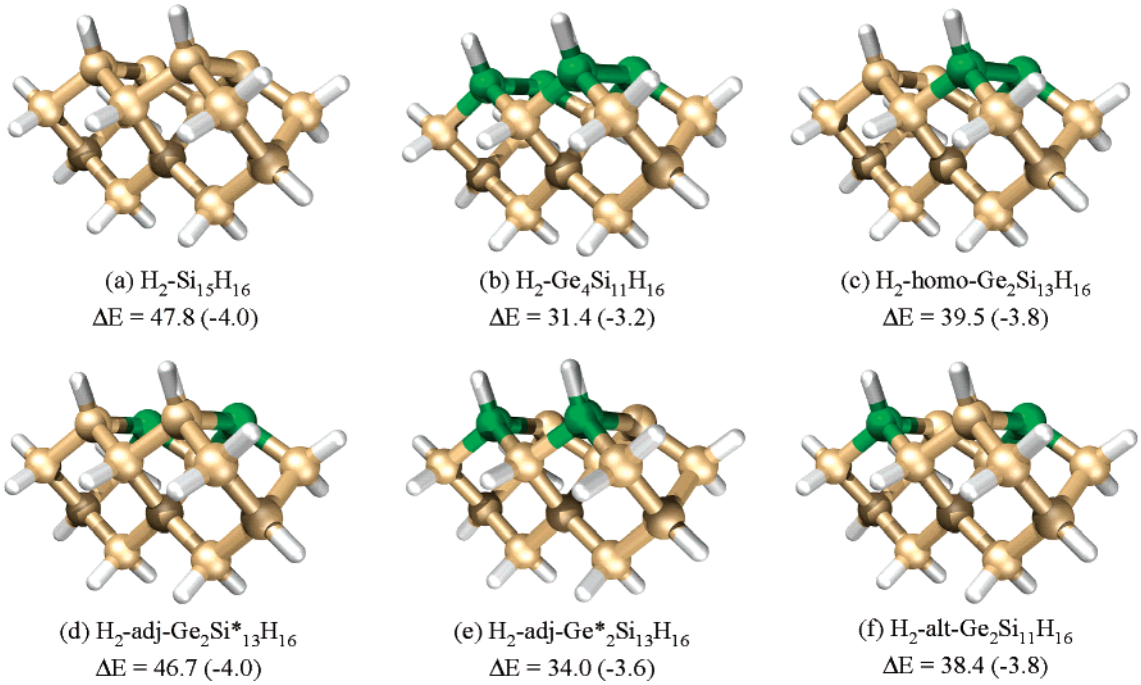

Figure 7. Optimized structures of two-dimer clusters with two hydrogen adsorbed on adjacent dimers: (a) $H_2-Si_{15}H_{16}$; (b) $H_2-Ge_4Si_{11}H_{16}$; (c) homo-$H_2-Ge_2Si_{13}H_{16}$; (d) adj-$H_2-Ge_2Si^*_{13}H_{16}$; (e) adj-$H_2-Ge^*_2Si_{13}H_{16}$; (f) alt-$H_2-Ge_2Si_{13}H_{16}$. The asterisk denotes the surface atoms with adsorbed hydrogens.

follow the order 4H > 3H > 2H, and desorption via the 3H interdimer mechanism and the prepairing mechanism have similar reaction energies.

2. Barrierless Hydrogen Adsorption via the 4H Mechanism. We have performed transition state searches for hydrogen desorption via the 4H interdimer mechanism to calculate the activation barrier for hydrogen desorption. However, we could not locate transition states for the hydrogen desorption process, despite intensive transition state searches. We conclude that the activation barrier for 4H interdimer desorption does not differ significantly from the energy of desorption. Therefore, there are three distinct activation barriers for hydrogen desorption from SiGe alloy surfaces via the 4H interdimer pathway, namely hydrogen desorption from two adjacent Si atoms (59.9 kcal/mol), desorption from two adjacent Ge atoms (46.9 kcal/mol), and desorption from two adjacent Si and Ge atoms (53.5 kcal/mol).

If the activation barrier for hydrogen desorption via the 4H pathway is equal to the endothermicity of the surface reaction, hydrogen *adsorption* via the 4H pathway must be barrierless. To show that there is no significant barrier to hydrogen *adsorption* via the 4H pathway, we performed energy minimization calculations to mimic the adsorption processes. Specifically, a hydrogen molecule is constrained at a relatively large distance from the surface with two hydrogen atoms adsorbed to neighboring dimers in adjacent positions, and the system is relaxed to minimize the energy. The barrierless *adsorption* reaction paths on unconstrained $H_2-Si_{15}H_{16}$ and $H_2-Ge_4Si_{11}H_{16}$ clusters are shown in Figure 8. On the $H_2-Si_{15}H_{16}$ cluster, the hydrogen molecule is placed 3.35 Å from the surface (Si−H = 3.75 Å), and a symmetric *adsorption* pathway was found. The reaction pathway is completely downhill in energy. A barrierless symmetric reaction path was also found for hydrogen adsorption on the $H_2-Ge_4Si_{11}H_{16}$ cluster, where the hydrogen molecule is placed 3.34 Å from the surface (Ge−H = 3.77 Å) initially.

We note that our calculations can only suggest but not confirm a barrierless pathway for 4H hydrogen adsorption. First, if the adsorption activation barrier is too small, the transition state search algorithm may not locate the transition state on the relatively flat potential energy surface. Second, close inspection of the barrierless adsorption pathways show that significant relaxations of the clusters occur during the adsorption process. On an actual surface, the subsurface atoms are constrained by bulk atoms. A small barrier to adsorption may exist on an actual surface but not on a completely relaxed cluster. Nevertheless, our calculations imply that the 4H adsorption process has an insignificant barrier, and therefore the desorption energy gives a good approximation to the activation barrier of hydrogen desorption via the 4H mechanism.

3. Transition States for Hydrogen Desorption via the 3H and 2H Mechanisms. The calculated activation barriers for hydrogen desorption via the 3H interdimer mechanism on unconstrained $Si_{15}H_{16}$ and $Ge_4Si_{11}H_{16}$ two-dimer clusters are 61.8 and 49.8 kcal/mol, respectively (Figure 9). We find that the activation barrier for hydrogen desorption from the $Si_{15}H_{16}$ two-dimer clusters via the 4H mechanism is lower than that via the 3H mechanism, which is in turn lower than the 2H barrier. In particular, the activation barrier for 4H, 3H, and 2H interdimer desorption from the $Si_{15}H_{16}$ two-dimer cluster are 59.9, 61.8, and 63.3 kcal/mol, respectively. However, the same trend is not observed on the $Ge_4Si_{11}H_{16}$ cluster. Specifically, the activation barrier for 4H, 3H, and 2H interdimer desorption are 46.9, 49.8, and 46.3 kcal/mol, respectively.

Optimized transition state structures for 2H interdimer desorption are shown in Figures 10 and 11, and the 2H activation barriers follow the order: $H_2^{\ddagger}-Si_{15}H_{16}$ (63.3 kcal/mol) > adj-$H_2^{\ddagger}-Ge_2Si^*_{13}H_{16}$ (58.2 kcal/mol) > alt-$H_2^{\ddagger}-Ge_2Si^*_{13}H_{16}$ (56.8 kcal/mol) > homo-$H_2^{\ddagger}-Ge^*_2Si_{13}H_{16}$ (55.0 kcal/mol) > homo-$H_2^{\ddagger}-Ge_2Si^*_{13}H_{16}$ (52.9 kcal/mol) > alt-$H_2^{\ddagger}-Ge^*_2Si_{13}H_{16}$ (52.0 kcal/mol) > adj-$H_2^{\ddagger}-Ge^*_2Si_{13}H_{16}$ (51.2 kcal/mol) > $H_2^{\ddagger}-Ge_4Si_{11}H_{16}$ (46.3 kcal/mol). Our calculations show that the activation barriers for 2H desorption are affected by both the occupied and unoccupied dimer atoms of the two dimer cluster. In addition, we find that the 2H activation barriers for hydrogen

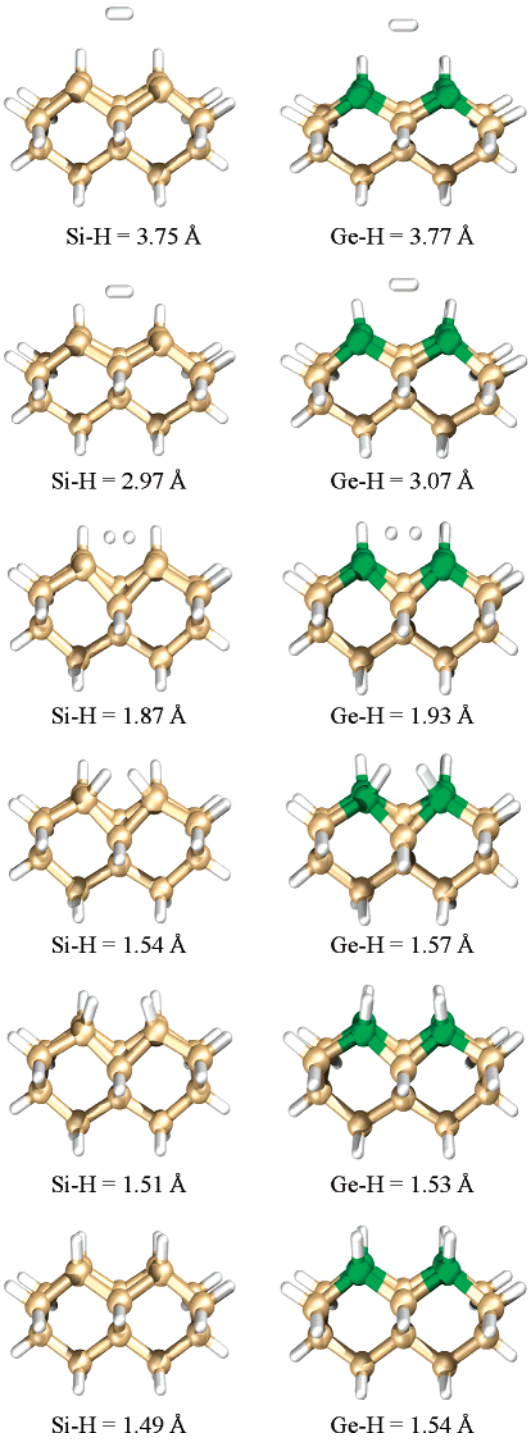

Figure 8. Barrierless pathways for hydrogen adsorption onto the $H_2-Si_{15}H_{16}$ (left) and $H_2-Ge_4Si_{11}H_{16}$ (right) clusters via the 4H interdimer mechanism.

desorption from adjacent Si and Ge atoms lie between those of desorption from adjacent Si and adjacent Ge atoms. This is in contrast to the effect of surface Ge atoms on the prepairing mechanisms, where the calculated activation barriers are affected by occupied dimer atoms only.

C. Effects of Neighboring Ge Atoms. *1. Prepairing Mechanism.* We use the Ge_9H_{12} one-dimer cluster to investigate the effect of bulk Ge atoms on the energetics of hydrogen desorption from SiGe alloy surfaces via the prepairing mechanism (Figure 12). The endothermicity for hydrogen desorption from the Ge_9H_{12} cluster is 41.3 kcal/mol, and the activation barrier for hydrogen desorption is 63.3 kcal/mol. Similarly, the endothermicity and activation barrier of hydrogen desorption on the $Ge_2Si_7H_{12}$ one-dimer cluster are 41.6 and 64.3 kcal/mol, respectively (Figure 12a). Therefore, bulk Ge atoms only have a minor effect on hydrogen desorption from SiGe alloy surfaces.

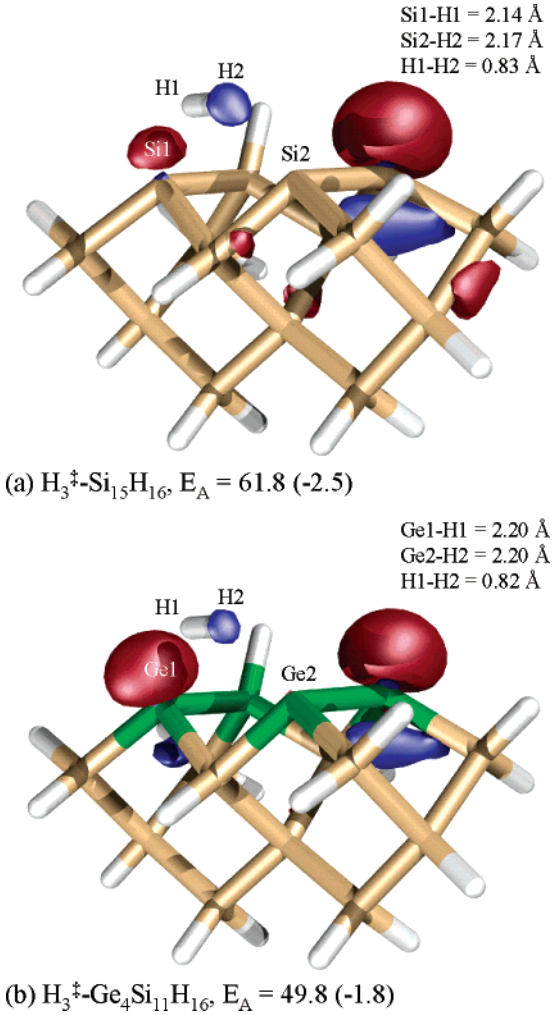

Figure 9. HOMOs of the transition states of hydrogen desorption from the Si(100)-2×1 and Ge/Si(100)-2×1 surfaces via the 3H interdimer mechanism: (a) $H_3^{\ddagger}-Si_{15}H_{16}$; (b) $H_3^{\ddagger}-Ge_4Si_{11}H_{16}$. The numbers in parentheses are zero-point corrections.

The $Ge_6Si_{15}H_{20}$ three-dimer cluster, for which the six surface atoms are occupied by three Ge−Ge dimers, is used to study the effects of neighboring surface Ge atoms on the calculated activation barrier. Our calculations on the $Ge_6Si_{15}H_{20}$ cluster show a reaction energy of 33.5 kcal/mol and an activation barrier of 53.4 kcal/mol, whereas the reaction energy and activation barrier on the $Ge_2Si_{19}H_{20}$ three-dimer cluster are 35.6 and 55.3 kcal/mol (Figure 12b). Thus, replacing Si by Ge atoms on the neighboring dimers decreases the reaction energy and activation barrier of hydrogen desorption from SiGe alloy surfaces by only 2 kcal/mol. Consequently, the nonlocal electronic effects of neighboring Ge dimer atoms are minor compared to the local effects of Ge dimer atoms on hydrogen desorption via the prepairing mechanism.

2. Interdimer Mechanisms. We use the $Ge_4Si_{23}H_{24}$ and $Ge_8Si_{19}H_{24}$ four-dimer clusters to investigate the effect of neighboring surface Ge atoms on the energetics of interdimer mechanisms, and we observe similar desorption reaction energies calculated on the two clusters (Figure 13). The calculated 4H, 3H, and 2H interdimer desorption reaction energies on the $Ge_4Si_{23}H_{24}$ cluster are calculated to be 45.7, 36.9, and 26.2 kcal/mol, respectively, whereas the corresponding desorption energies

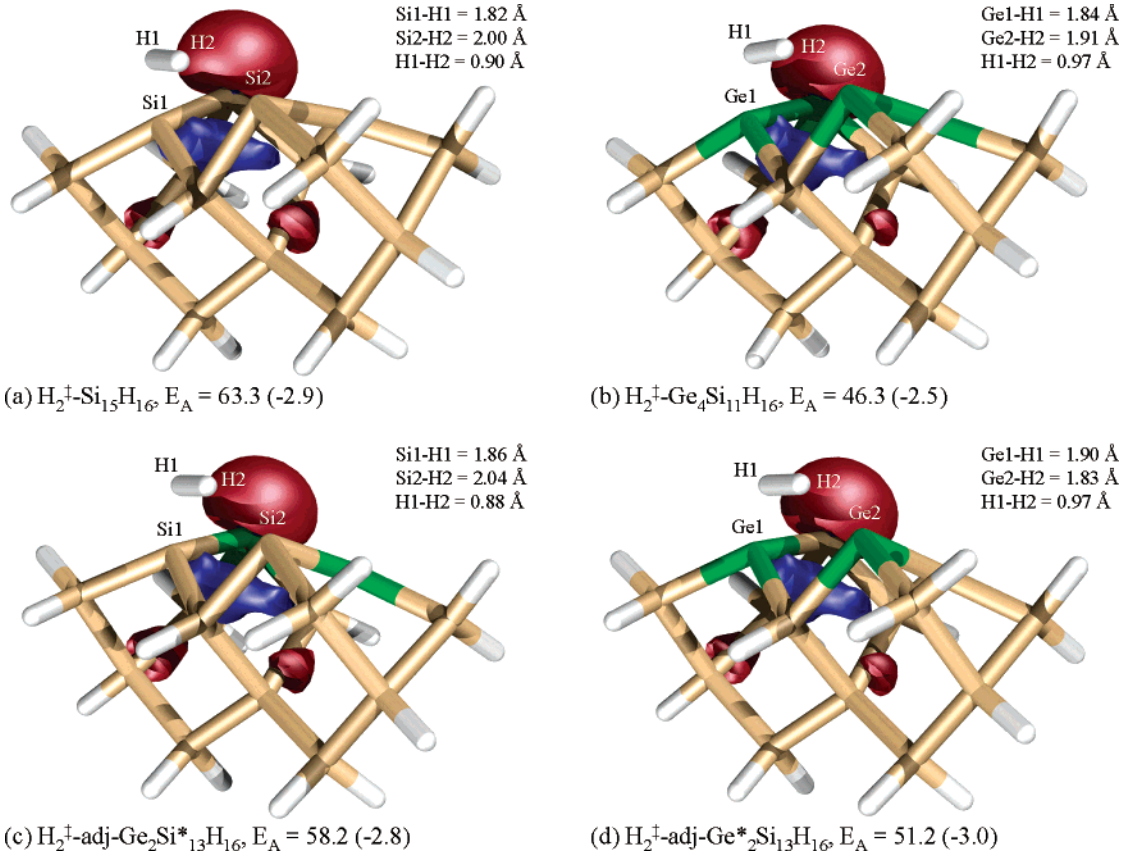

Figure 10. HOMOs of the transition states of hydrogen desorption from identical adjacent surface atoms via the 2H interdimer mechanism: (a) $H_2^{\ddagger}-Si_{15}H_{16}$; (b) $H_2^{\ddagger}-Ge_4Si_{11}H_{16}$; (c) adj-$H_2^{\ddagger}-Ge_2Si^*_{13}H_{16}$; (d) adj-$H_2^{\ddagger}-Ge^*_2Si_{13}H_{16}$. The asterisk denotes the surface atoms from which hydrogen desorbs via the 2H mechanism. The numbers in parentheses are zero-point corrections.

TABLE 2: Energies (kcal/mol) of Recombinative Hydrogen Desorption from SiGe Alloy Dimers via the Prepairing Mechanism[a]

energies of H_2 desorption	Si−Si	Ge−Si	Ge−Ge
one-dimer unconstrained	53.9	47.8	41.6
one-dimer constrained	51.9	43.6	37.1
three-dimer unconstrained	52.0	43.2	35.6
three-dimer constrained	50.7		32.7[b]
zero point correction	−3.8	−3.7	−3.5

[a] The asterisk denotes the up atom of the dimer. The energies of hydrogen desorption on the Ge−Si heterodimer are relative to the Ge*−Si dimer cluster. The zero point corrections are calculated from unconstrained one-dimer clusters. [b] Calculated on the constrained $Ge_6Si_{15}H_{20}$ three-dimer cluster.

TABLE 3: Activation Barriers (kcal/mol) of Recombinative Hydrogen Desorption from SiGe Alloy Dimers via the Prepairing Mechanism.

activation barrier of H_2 desorption	Si−Si	Ge−Ge	Ge−Si*	Ge*−Si
one-dimer unconstrained	74.1	64.3	74.2	64.0
one-dimer constrained	71.2	61.4	71.9	60.3
three-dimer unconstrained	66.2	55.3	66.0	55.6
three-dimer constrained	64.8	52.4[a]		
zero point correction	−2.1	−2.4	−2.7	−2.0

[a] Calculated on the constrained $Ge_6Si_{15}H_{20}$ three-dimer cluster.

on the $Ge_8Si_{19}H_{24}$ cluster are 45.9, 35.8, and 24.3 kcal/mol, respectively. The activation barriers calculated using the two clusters are also similar. The 2H and 3H activation barriers on the $Ge_4Si_{23}H_{24}$ cluster are calculated to be 40.1 and 47.7 kcal/mol, respectively, and the corresponding barriers on the $Ge_8Si_{19}H_{24}$ cluster are 38.9 and 47.0 kcal/mol, respectively. We find that the neighboring surface Ge atoms decrease the reaction energy and activation barrier for hydrogen desorption via interdimer mechanisms only slightly.

D. Cluster Size Effects. *1. Prepairing Mechanism.* Calculations on three-dimer clusters are performed to determine the effect of cluster size on the reaction energies and activation barriers of hydrogen desorption from SiGe alloy dimers via the prepairing mechanism. Table 2 summarizes the reaction energies for hydrogen desorption via the prepairing mechanism calculated on different clusters. The HOMO of the transition state structures and activation barriers on three-dimer clusters are shown in Figure 14. We find that the energy of recombinative hydrogen desorption decreases when three-dimer clusters are used (Table 2). Furthermore, this cluster size effect increases when Ge atoms are present on the surface. Specifically, the energy of hydrogen desorption from the $Si_{21}H_{20}$, $GeSi_{20}H_{20}$, and $Ge_2Si_{19}H_{20}$ three-dimer clusters decreases by 2.0, 4.6, and 5.9 kcal/mol, respectively.

We observe a larger cluster size effect on the activation barriers than on the reaction energies for hydrogen desorption from SiGe alloy dimers. The activation barriers calculated using unconstrained Si−Si, Ge−Ge, Ge−Si*, and Ge*−Si three-dimer clusters are 66.2, 55.3, 66.0, and 55.6 kcal/mol, respectively (Figures 14a−d). Specifically, the activation barriers on unconstrained Si−Si, Ge−Ge, Ge−Si*, and Ge*−Si three-dimer clusters decrease by 7.9, 9.0, 8.2, and 8.4 kcal/mol, respectively, compared to the barriers calculated on one-dimer clusters (Table 3). The cluster size effect on activation barriers is due to charge transfer from the desorbing hydrogen at the transition state to the empty neighboring dimers. For the one-dimer clusters, the electron density from the prepaired hydrogen atoms is transferred to the up atom of the dimers, as evident in the HOMO diagrams (Figure 4). On the three-dimer clusters, the HOMO

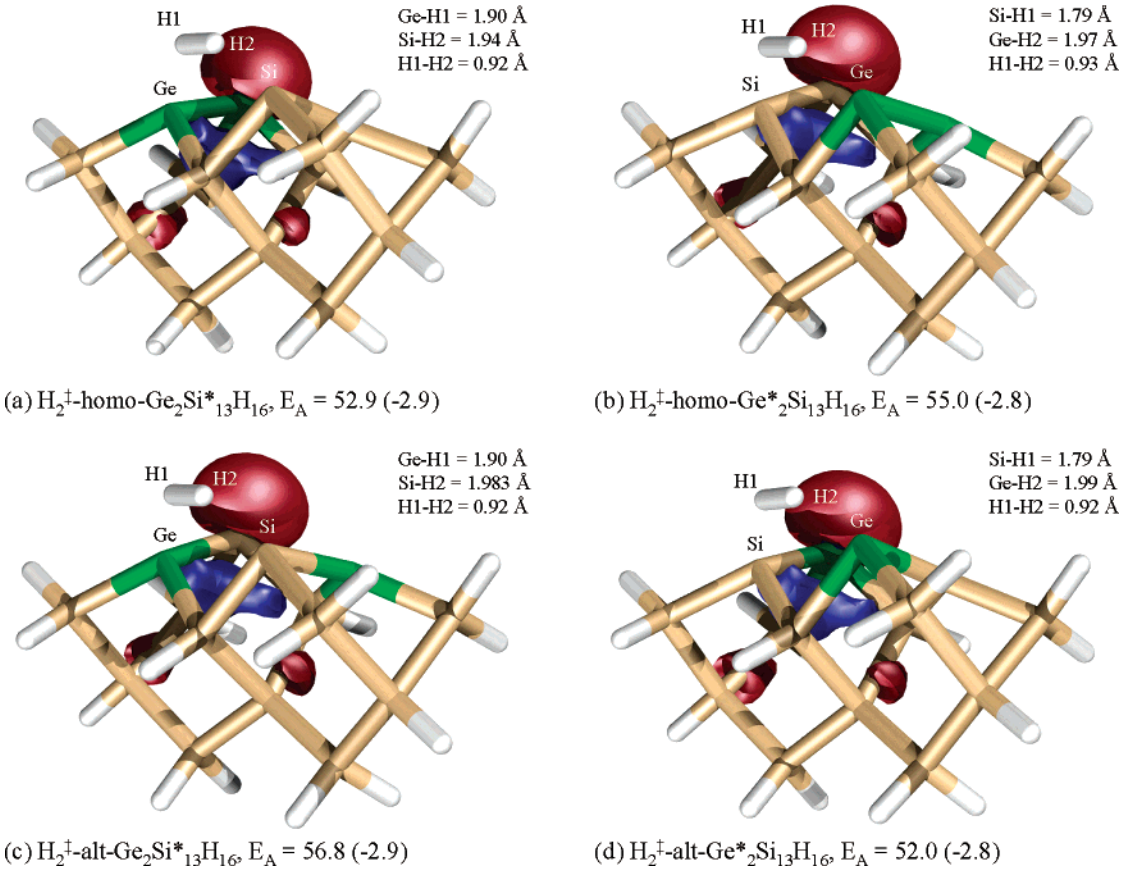

Figure 11. HOMOs of the transition states of hydrogen desorption from different adjacent surface atoms via the 2H interdimer mechanism: (a) homo-$H_2^{\ddagger}-Ge_2Si^*_{13}H_{16}$; (b) homo-$H_2^{\ddagger}-Ge^*_2Si_{13}H_{16}$; (c) alt-$H_2^{\ddagger}-Ge_2Si^*_{13}H_{16}$; (d) adj-$H_2^{\ddagger}-Ge^*_2Si_{13}H_{16}$. The asterisk denotes the up atom from which hydrogen desorbs via the 2H mechanism. The numbers in parentheses are zero point corrections.

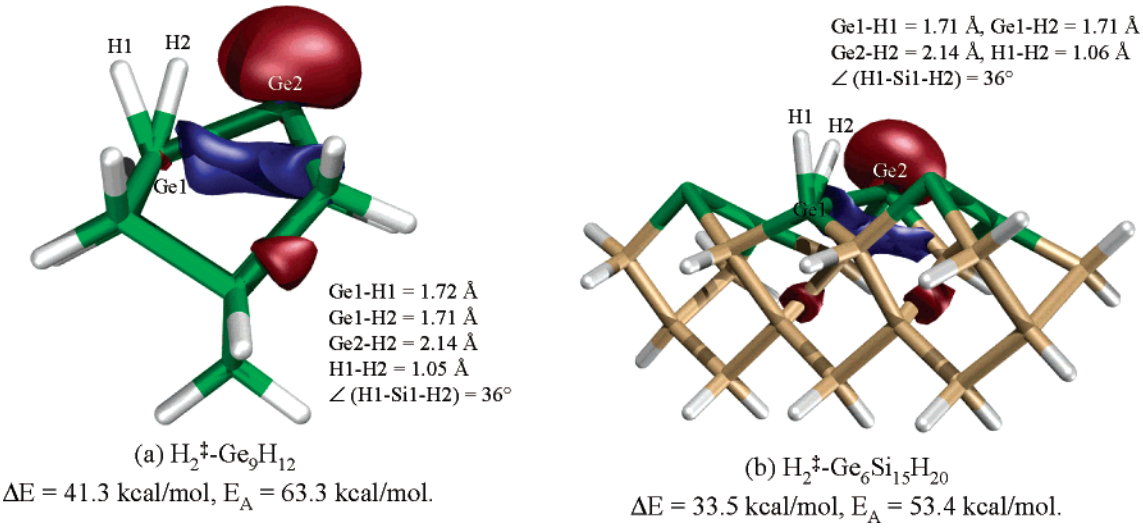

Figure 12. Transition state HOMOs to illustrate the effects of bulk and surface Ge atoms on hydrogen desorption: (a) $H_2^{\ddagger}-Ge_9H_{12}$; (b) $H_2^{\ddagger}-Ge_6Si_{15}H_{20}$.

diagrams show that the electron density extends to the up atoms of neighboring dimers at the transition state. This charge-transfer effect stabilizes the transition states on three-dimer clusters, lowering the calculated activation barriers (Figures 14a−d).

To further investigate the origin of the charge-transfer effect, we calculated the activation barrier of hydrogen desorption from a $H_2^{\ddagger}-Si_{21}H_{24}$ three-dimer cluster, on which six hydrogen atoms occupy all three dimers of the cluster (Figure 14e). We find that the activation barrier for hydrogen desorption from the central dimer is 71.4 kcal/mol, whereas the desorption barrier obtained from the $H_2^{\ddagger}-Si_9H_{12}$ one-dimer cluster calculation is 74.1 kcal/mol. This is because the π^* orbitals on the neighboring dimers, to which charge transfers on the clean surface, become Si−H bonds on the hydrogen terminated surface and thus are energetically unavailable to accept charge. As a consequence, the additional electron density from the two hydrogen atoms at the transition state can only transfer to the up atom of the central dimer and the energy of the transition state on the $H_2^{\ddagger}-Si_{21}H_{24}$ cluster is increased. The HOMO of the transition state with H passivation is thus similar to that of the Si_9H_{12} one-dimer cluster (Figures 4a and 14e).

Similar cluster size effects have been observed in DFT

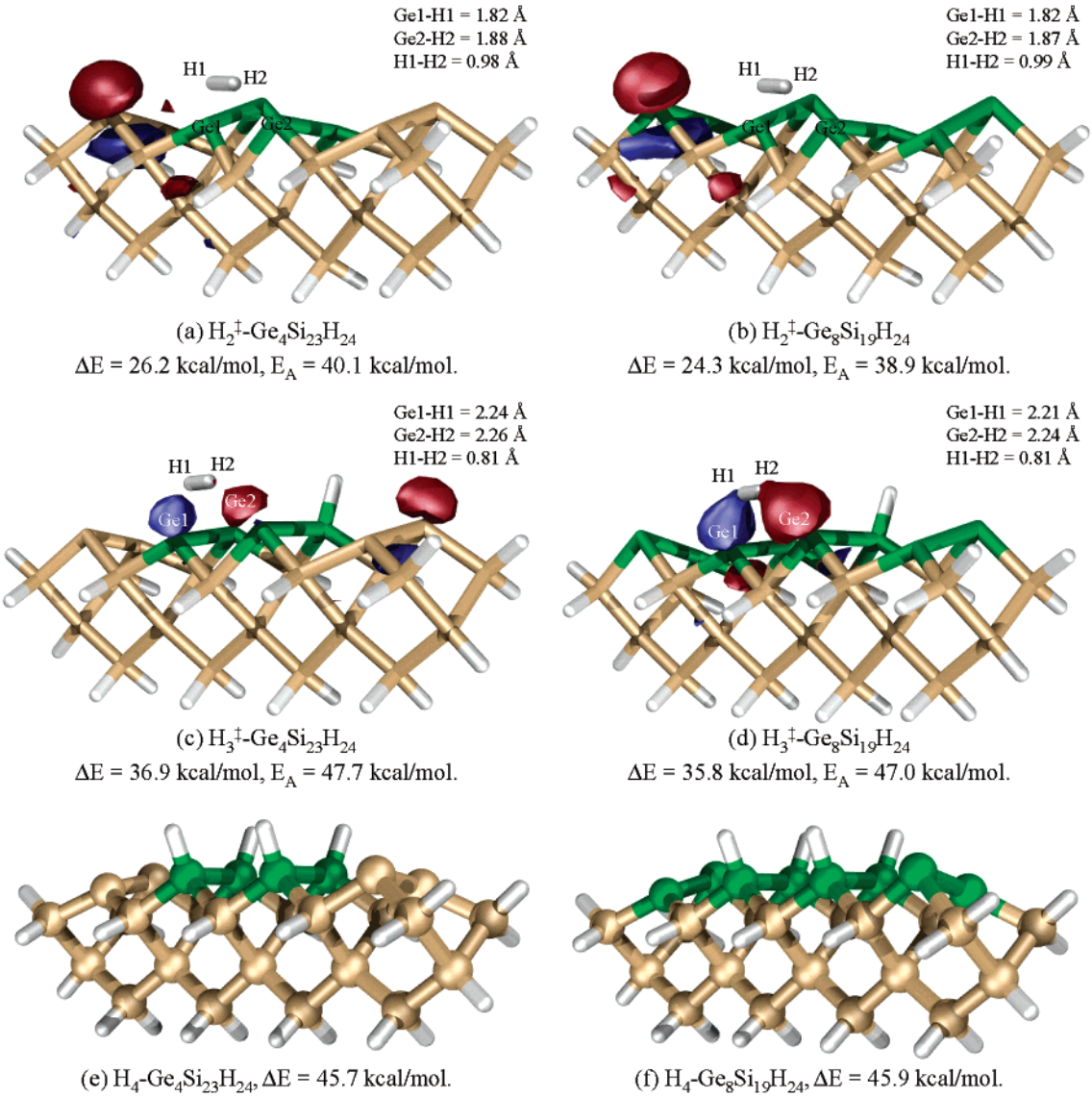

Figure 13. Transition state HOMOs and stable structures on four-dimer clusters to illustrate the effect of surface Ge atoms on hydrogen desorption via interdimer mechanisms: (a) $H_2^{\ddagger}-Ge_4Si_{23}H_{24}$; (b) $H_2^{\ddagger}-Ge_8Si_{19}H_{24}$; (c) $H_3^{\ddagger}-Ge_4Si_{23}H_{24}$; (d) $H_3^{\ddagger}-Ge_8Si_{19}H_{24}$; (e) $H_4-Ge_4Si_{23}H_{24}$; (f) $H_4-Ge_8Si_{19}H_{24}$.

calculations of hydrogen desorption from the Si(100)-2×1 surface.[57,61,71] In addition, Widjaja and Musgrave also observed cluster size effects resulting from charge transfer from the lone pair of an adsorbing ammonia molecule to the Si(100)-2×1 surface.[72] Our calculations show that this charge-transfer effect also applies to transition state structures of hydrogen desorption, where the extra electron density is donated by the two hydrogen atoms prepaired above the down atom of the dimer at the transition state.

2. Interdimer Mechanisms. To investigate whether charge transfer affects the energetics of the interdimer mechanisms, we use the $Si_{27}H_{24}$, $Si_{27}H_{28}$, and $Ge_4Si_{23}H_{24}$ four-dimer clusters. The energies are summarized in Tables 4 and 5, and optimized structures calculated on the $Si_{27}H_{24}$ and $Si_{27}H_{28}$ clusters are shown in Figure 15. We find that the reaction energy of hydrogen desorption decreases with neighboring Si−Si dimers, but the effects are moderate. In particular, the 2H, 3H, and 4H desorption energies calculated on the unconstrained $Si_{27}H_{24}$ four-dimer cluster are 44.7, 52.4, and 59.3 kcal/mol, respectively, which are 3.1, 1.4, and 0.6 kcal/mol lower than the reaction energies calculated on the $Si_{15}H_{16}$ two-dimer cluster (Table 4). Similarly, the 2H, 3H, and 4H desorption energies calculated on unconstrained $Ge_4Si_{23}H_{24}$ four-dimer cluster are 5.2, 3.2, and 1.2 kcal/mol lower than the corresponding energies on the $Ge_4Si_{11}H_{16}$ two-dimer cluster (Table 5).

We find that the activation barriers of 2H and 3H desorption decrease when four-dimer clusters are used, and the cluster size effect on activation barriers is larger than that on reaction energies. Specifically, the 2H and 3H activation barriers calculated on the unconstrained $Si_{27}H_{24}$ four-dimer cluster are 56.6 and 60.5 kcal/mol, respectively, which are 7.3 and 1.3 kcal/mol lower than those calculated on unconstrained $Si_{15}H_{16}$ cluster (Table 4). On the $Ge_4Si_{23}H_{24}$ cluster, the calculated 2H and 3H activation barriers are 6.2 and 2.1 kcal/mol lower than those calculated on the $Ge_4Si_{11}H_{16}$ cluster (Table 5). In addition, inspection of the HOMO diagrams reveal that the 2H and 3H transition states have significant electron density on the nucleophilic up atom on the neighboring dimers, confirming the charge-transfer effect during hydrogen desorption via interdimer mechanisms (Figures 13 and 15). We also find that cluster size effects are larger on the calculated activation barrier of the 2H

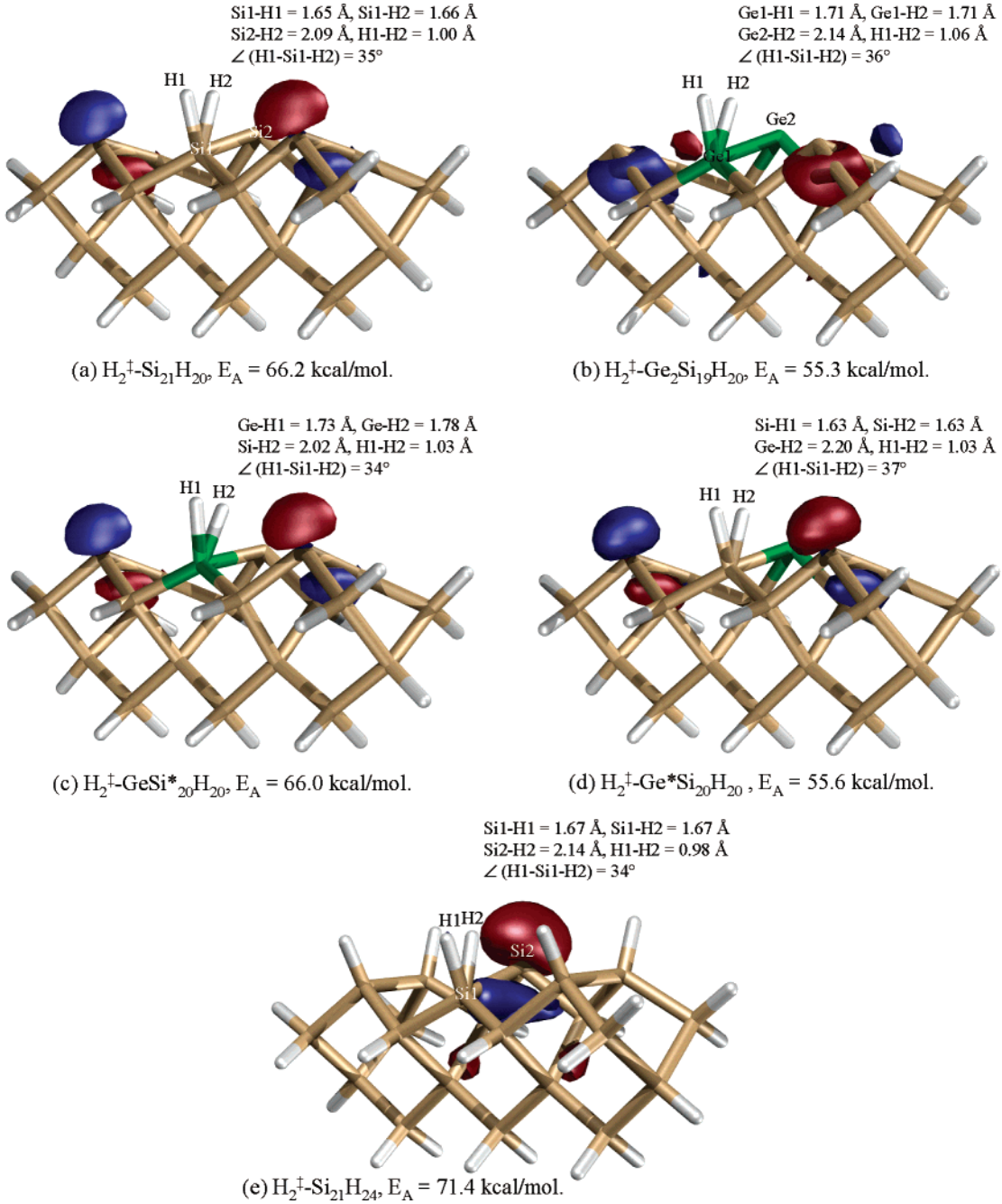

Figure 14. HOMOs of the transition state structures on three-dimer clusters: (a) $H_2^{\ddagger}-Si_{21}H_{20}$; (b) $H_2^{\ddagger}-Ge_2Si_{19}H_{20}$; (c) $H_2^{\ddagger}-GeSi^*_{20}H_{20}$; (d) $H_2^{\ddagger}-Ge^*Si_{20}H_{20}$; (e) $H_2^{\ddagger}-H_4-Si_{21}H_{20}$.

TABLE 4: Reaction Energies and Activation Barriers (kcal/mol) of Hydrogen Desorption from Two Adjacent Si−Si Homodimers via Interdimer Mechanisms[a]

adjacent Si−Si dimers	ΔE (4H)	ΔE (3H)	ΔE (2H)	E_A (3H)	E_A (2H)
$Si_{15}H_{16}$ unconstrained	59.9	53.8	47.8	61.8	63.3
$Si_{15}H_{16}$ constrained	59.8	53.7	47.0	64.8	69.3
$Si_{27}H_{24}$ unconstrained	59.3	52.4	44.7	60.5	56.0
$Si_{27}H_{24}$ constrained	59.5	52.3	43.6	62.0	61.2
$Si_{27}H_{28}$ unconstrained	59.4	54.1	46.1	60.6	59.2
zero point correction	−3.9	−3.9	−4.0	−2.5	−2.9

[a] The zero point corrections are calculated from unconstrained two-dimer clusters.

TABLE 5: Reaction Energies and Activation Barriers (kcal/mol) of Hydrogen Desorption from Two Adjacent Ge−Ge Homodimers via Interdimer Mechanisms

adjacent Ge−Ge dimers	ΔE (4H)	ΔE (3H)	ΔE (2H)	E_A (3H)	E_A (2H)
$Ge_4Si_{11}H_{16}$ unconstrained	46.9	40.1	31.4	49.8	46.3
$Ge_4Si_{11}H_{16}$ constrained	47.0	38.9	28.7	52.4	52.6
$Ge_4Si_{23}H_{24}$ unconstrained	45.7	36.9	26.2	47.7	40.1
$Ge_8Si_{19}H_{24}$ unconstrained	45.9	35.8	24.3	47.0	38.9
$Ge_8Si_{19}H_{24}$ constrained	46.4	35.7	22.6	48.8	43.6
zero point correction	−4.0	−3.6	−3.2	−1.8	−2.5

interdimer mechanism, which indicates that 2H desorption involves larger charge-transfer effects than 3H desorption.

We use the $Si_{27}H_{28}$ four-dimer cluster to investigate the origin of the charge-transfer effect on the activation barrier of hydrogen desorption via interdimer mechanisms. The $H_2^{\ddagger}-Si_{27}H_{28}$ four-dimer cluster has eight hydrogen atoms that occupy all four dimers on the cluster. Similar to the $H_2^{\ddagger}-Si_{21}H_{24}$ cluster, the π and π^* orbitals of the two neighboring dimers are replaced by Si−H bonds, and charge transfer during hydrogen desorption to π^* orbitals of the neighboring bare dimers is prevented. Therefore, the HOMO diagrams of the 2H and 3H transition

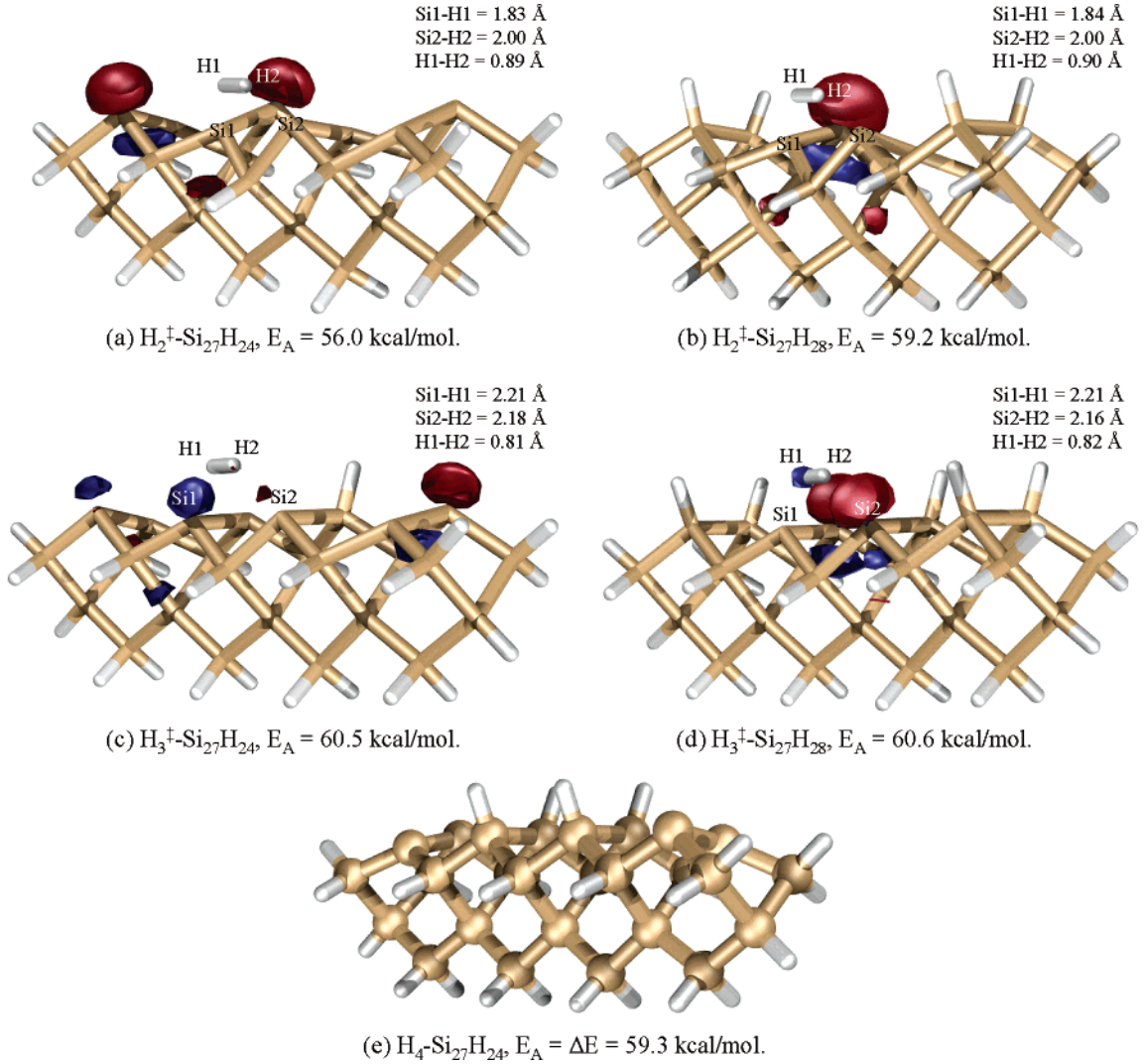

Figure 15. Comparison of transition state HOMOs on the $Si_{27}H_{24}$ three-dimer cluster to illustrate charge-transfer effects: (a) $H_2^{\ddagger}-Si_{27}H_{24}$; (b) $H_2^{\ddagger}-Si_{27}H_{28}$; (c) $H_3^{\ddagger}-Si_{27}H_{24}$; (d) $H_3^{\ddagger}-Si_{27}H_{28}$; (e) $H_4-Si_{27}H_{24}$.

states on the $Si_{27}H_{24}$ four-dimer cluster are similar to the HOMO diagrams calculated on the $Si_{15}H_{16}$ two-dimer cluster (Figures 9, 10, and 15). However, our calculations show that electron donation to neighboring dimers can only partially account for the cluster size effect on the calculated activation barriers for interdimer hydrogen desorption. In particular, the calculated 2H activation barrier on the $H_2^{\ddagger}-Si_{27}H_{24}$ four-dimer cluster is 7.3 kcal/mol lower than that on the $H_2^{\ddagger}-Si_{15}H_{16}$ two-dimer cluster. On the other hand, the calculated 2H activation barrier on the $H_2^{\ddagger}-Si_{27}H_{28}$ cluster is 3.2 kcal/mol higher than that on the $H_2^{\ddagger}-Si_{27}H_{24}$ cluster. Although charge transfer to neighboring dimers is largely diminished on either the $H_2^{\ddagger}-Si_{15}H_{16}$ two-dimer or $H_2^{\ddagger}-Si_{27}H_{28}$ four-dimer clusters, the activation barriers calculated on the two clusters are different. We attribute the difference in activation barriers calculated on the two cluster systems to the difference in strain environments in the $H_2^{\ddagger}-Si_{15}H_{16}$ two-dimer and $H_2^{\ddagger}-Si_{27}H_{24}$ four-dimer clusters.

E. Effect of Constraints. *1. Prepairing Mechanism.* Constraints are frequently imposed on cluster models to prevent unrealistic relaxation of the bulk atoms, as well as to mimic the actual surface strain of chemical reactions. Because the cluster has a finite size, imposing constraints on the cluster does not necessarily reproduce the elastic strain from the bulk atoms accurately. However, constrained cluster calculations usually provide more realistic estimates on the surface reaction energies and activation barriers, especially when the unconstrained cluster calculations result in unrealistic relaxations. For the case of hydrogen desorption from the Si(100)-2×1 surface via the prepairing mechanism, calculations on the unconstrained clusters do not result in large relaxations. Therefore, we use this surface reaction as an example to illustrate the combined effects of constraints and cluster size.

Our calculations on constrained one-dimer clusters lead to lower reaction energies and activation barriers for hydrogen desorption on SiGe dimers. Specifically, although the desorption energies on *unconstrained* Si−Si, Ge−Si, and Ge−Ge one-dimer clusters are 53.9, 47.8, and 41.6 kcal/mol, respectively, the corresponding energies on *constrained* one-dimer clusters are 51.9, 43.6, and 37.1 kcal/mol, respectively. The desorption energies on the *unconstrained* and *constrained* $Si_{21}H_{20}$ three-dimer clusters are calculated to be 52.0 and 50.7 kcal/mol, respectively (Table 2). In addition, we find that the effect of constraints decreases with increasing cluster size. For example, the hydrogen desorption energy on the *constrained* $Ge_2Si_7H_{12}$ one-dimer cluster is 4.5 kcal/mol lower than on the *unconstrained* $Ge_2Si_7H_{12}$ cluster, whereas the difference decreases by only 0.8 kcal/mol when constraints are imposed on the $Ge_6Si_{15}H_{20}$ three-dimer cluster (Table 2).

The effect of constraints on the activation barrier for hydrogen desorption via the prepairing mechanism from SiGe alloy

surfaces also decreases with increasing cluster size. Though the calculated activation barriers for hydrogen desorption from unconstrained $H_2^{\ddagger}-Si_9H_{12}$ and $H_2^{\ddagger}-Si_{20}H_{21}$ clusters are 74.1 and 66.2 kcal/mol, respectively, the activation barriers on *constrained* one and three-dimer clusters are 71.2 and 64.8 kcal/mol. For hydrogen desorption from the Ge−Ge dimer, the difference in activation barriers on the *constrained* and *unconstrained* $H_2^{\ddagger}-Ge_2Si_7H_{12}$ one-dimer clusters is 2.9 kcal/mol, and the effect of constraints decreases to 1.0 kcal/mol on the $H_2^{\ddagger}-Ge_6Si_{15}H_{20}$ three-dimer cluster (Table 3).

The combined effect of constraints and cluster size on hydrogen desorption via the prepairing mechanism implies that imposing constraints on the cluster is effective and important only when the clusters are small, because the effect of constraints decreases as the cluster size increases. However, constrained geometry optimization becomes the only option when unrealistic relaxations occur during optimization. For hydrogen desorption from SiGe alloy surfaces via the prepairing mechanism, one effect of constraints originates from the fact that the terminating Si−H bonds are stiffer than the bulk Si−Si bonds they represent. Constraining the positions of the terminating hydrogens leads to more restricted movement of the bulk atoms in the cluster due to the stiffer Si−H termination. When the cluster size increases, some of the Si−H bonds close to the dimer on which reaction occurs are replaced by Si−Si bonds. Because the stiffer Si−H bonds are farther away from the dimer on which reaction occurs, the effect of imposing constraints on the calculated energetics decreases when three-dimer clusters are used.

2. Interdimer Mechanisms. Our calculations on constrained $Si_{15}H_{16}$ and $Ge_4Si_{11}H_{16}$ two-dimer clusters show that the energies of hydrogen desorption via interdimer mechanisms are not affected by geometric constraints imposed on the cluster (Table 4). Similar effects of constraints are observed when the calculated desorption energies on constrained and unconstrained $Ge_4Si_{11}H_{16}$ clusters are compared (Table 5).

Unlike the calculated desorption energies, we find that the calculated 3H and 2H activation barriers are affected by constraints imposed on the cluster. For example, the 3H activation barriers on the *constrained* $H_3^{\ddagger}-Si_{15}H_{16}$ and $H_{3\ddagger}-Ge_4Si_{11}H_{16}$ two-dimer clusters are 64.7 and 52.4 kcal/mol, respectively, whereas the corresponding activation barriers on the *unconstrained* $H_3^{\ddagger}-Si_{15}H_{16}$ and $H_3^{\ddagger}-Ge_4Si_{11}H_{16}$ clusters are 61.8 and 49.8 kcal/mol. The effect of constraints is particularly prominent in calculated barriers for the 2H interdimer mechanism. The 2H activation barriers on the *constrained* $H_2^{\ddagger}-Si_{15}H_{16}$ and $H_2^{\ddagger}-Ge_4Si_{11}H_{16}$ clusters are 69.3 and 52.6 kcal/mol, respectively. In other words, the 2H activation barriers increase by 6.0 and 6.3 kcal/mol when *constrained* $H_2^{\ddagger}-Si_{15}H_{16}$ and $H_2^{\ddagger}-Ge_4Si_{11}H_{16}$ two-dimer clusters are used, respectively. Inspection of the *unconstrained* $H_2^{\ddagger}-Si_{15}H_{16}$ and $H_2^{\ddagger}-Ge_4Si_{11}H_{16}$ 2H transition states structures reveals noticeable distortion of the clusters, such that even the bottom layer Si atoms are displaced from their crystallographic positions. Imposing constraints on the cluster increases the energy of the transition state, because there are fewer geometric degrees of freedom for energy minimization. On the other hand, the energy minima of the *unconstrained* $H_2-Si_{15}H_{16}$ and $H_4-Si_{15}H_{16}$ clusters do not involve significant geometric relaxation. Hence imposing constraints on them has a negligible effect on the calculated desorption energies.

Similar to the prepairing mechanism, we find that the effect of constraints on the calculated energetics for the interdimer mechanisms decreases when larger clusters are used. According to our calculations, the 2H and 3H activation barriers increase by 6.0 and 3.0 kcal/mol, respectively, when constraints are imposed on the $Si_{15}H_{16}$ two-dimer cluster, whereas the corresponding differences decrease to 5.2 and 1.5 kcal/mol, respectively, on the $Si_{27}H_{24}$ four-dimer cluster (Table 4). The combined effects of constraints and cluster size on hydrogen desorption from adjacent Ge−Ge homodimers via interdimer mechanisms are shown in Table 5, where similar energetic trends can be observed when the calculated activation barriers on constrained and unconstrained $Ge_4Si_{11}H_{16}$ two-dimer clusters are compared with those calculated on constrained and unconstrained $Ge_8Si_{19}H_{24}$ four-dimer clusters. However, due to the geometric distortion involved in the 2H transition states, the effect of constraints on the calculated 2H activation barriers on $Si_{27}H_{24}$ and $Ge_8Si_{19}H_{24}$ four-dimer clusters are relatively large compared to that observed for 3H desorption, the transition states of which do not involve significant geometric distortions. This shows that merely increasing the cluster size does not alleviate the effect of geometric distortion on the calculated energetics, and it is necessary to impose constraints on systems in which unrealistic geometric distortions are expected.

F. Comparison of Prepairing and Interdimer Mechanisms. Whereas there is only one single pathway for hydrogen desorption via the prepairing mechanism, there are three interdimer pathways for hydrogen desorption. Despite the number of possible pathways in the prepairing and interdimer mechanisms, the most notable difference between the two mechanisms is the effect of surface Ge on the desorption activation barriers. For the prepairing mechanism, the effect of surface Ge on the desorption process is local in nature, and the activation barrier is only affected by the identity of the up atom of the transition state. As a result, there are two distinct values for the activation barriers. On the other hand, the activation barrier for 2H desorption is affected by all four surface atoms on the two dimer cluster. This results in a range of values for the activation barriers of the 2H mechanism.

When the calculated activation barriers of the two mechanisms are compared, we find that the activation barriers for hydrogen desorption via the interdimer mechanisms are generally lower than those via the prepairing mechanism. For example, the activation barriers for hydrogen desorption via the 4H, 3H, and 2H interdimer mechanisms from the Si(100)-2×1 surface are 59.5 kcal/mol (constrained $H_4^{\ddagger}-Si_{27}H_{24}$), 62.0 kcal/mol (constrained $H_3^{\ddagger}-Si_{27}H_{24}$), and 61.2 kcal/mol (constrained $H_2^{\ddagger}-Si_{27}H_{24}$), whereas the activation barrier via the prepairing mechanism is 64.8 kcal/mol (constrained $H_2^{\ddagger}-Si_{21}H_{20}$). On the Ge/Si(100)-2×1 surface, the activation barriers for the 4H, 3H, and 2H interdimer and the prepairing mechanisms are 46.4 kcal/mol (constrained $H_4^{\ddagger}-Ge_8Si_{19}H_{24}$), 48.8 kcal/mol (constrained $H_3^{\ddagger}-Ge_8Si_{19}H_{24}$), 43.6 kcal/mol (constrained $H_2^{\ddagger}-Ge_8Si_{19}H_{24}$), and 52.4 kcal/mol (constrained $H_2^{\ddagger}-Ge_6Si_{15}H_{20}$), respectively. From the calculated activation barriers, our results indicate that the prepairing and the interdimer mechanisms may compete kinetically, especially at low coverages when the 2H and 3H interdimer mechanisms dominate.

The fact that the prepairing and interdimer mechanisms can compete kinetically suggests that the kinetics of hydrogen desorption from the Si(100)-2×1 and Ge(100)-2×1 surfaces are affected by both mechanisms. In fact, when the DFT-calculated activation barriers are incorporated into a statistical mechanical model for temperature programmed desorption, the simulated TPD spectra show discrepancies with experiments.[64]

IV. Conclusion

We have applied density functional theory with cluster models to study hydrogen desorption from SiGe alloy surfaces via both

the prepairing and interdimer mechanisms. For the prepairing mechanism, the calculations show that the activation barrier depends only on the identity of the up atom of the dimer. Therefore, there are only two distinct activation barriers for hydrogen desorption from the Si−Si, Ge*−Si, Ge−Si* and Ge−Ge dimers. Our calculations also show that neighboring Ge atoms, whether in the bulk or on neighboring dimers, have a minimal effect on the kinetics of hydrogen desorption via the prepairing mechanism. Furthermore, we found that whereas cluster size has a significant effect on the activation barrier for hydrogen desorption from SiGe alloy dimers, the effect of constraints is relatively minor, particularly with large clusters.

For hydrogen desorption via interdimer mechanisms, our calculations show that the 4H desorption barrier is not significantly higher than the 4H desorption energy. For the 2H pathway, our calculations show that the activation barrier for hydrogen desorption is affected by the presence of Ge atoms in all four positions of the adjacent dimers. Therefore, hydrogen desorption from SiGe alloy surfaces via the interdimer mechanism has a range of activation barriers. We also found that though the effects of cluster size and constraints are minimal on interdimer desorption energies, the calculated 2H activation barriers are affected by a combination of cluster size and constraints.

Acknowledgment. C.B.M. gratefully acknowledges the support of the Semiconductor Research Corporation Materials Structures and Devices MARCO Center, the Office of Naval Research, and Stanford's Center for Integrated Systems and Initiative for Nanoscale Materials Processing. S.F.B. acknowledges financial support from the National Science Foundation (CHE 9900041 and 0245260). This work was partially supported by the National Computational Science Alliance (NCSA).

References and Notes

(1) Whall, T. E.; Parker, E. H. C. *Thin Solid Films* **2000**, *367*, 250.
(2) Meyerson, B. S. *IBM J. Res., Dev.* **2000**, *44*, 391.
(3) Presting, H.; Konle, J.; Hepp, M.; Kibbel, H.; Thonke, K.; Sauer, R.; Corbin, E.; Jaros, M. *Opt. Eng.* **2000**, *39*, 2624.
(4) See, P.; Paul, D. J.; Hollander, B.; Mantl, S.; Zozoulenko, I. V.; Berggren, K. F. *IEEE Electron Dev. Lett* **2001**, *22*, 182.
(5) Arienzo, M.; Iyer, S. S.; Meyerson, B. S.; Patton, G. L.; Stork, J. M. C. *Appl. Surf. Sci.* **1991**, *48*−*49*, 377.
(6) Greve, D. W. *Mater. Sci. Eng. B* **1993**, *18*, 22.
(7) Joyce, B. A.; Fernandez, J. M.; Xie, M. H.; Matsumura, A.; Zhang, J.; Taylor, A. G. *J. Cryst. Growth* **1996**, *164*, 214.
(8) Meyerson, B. S.; Uram, K. J.; Legoues, F. K. *Appl. Phys. Lett.* **1988**, *53*, 2555.
(9) Hoyt, J. L.; King, C. A.; Noble, D. B.; Gronet, C. M.; Gibbons, J. F.; Scott, M. P.; Laderman, S. S.; Rosner, S. J.; Nauka, K.; Turner, J.; Kamins, T. I. *Thin Solid Films* **1990**, *184*, 93.
(10) Jang, S. M.; Reif, R. *Appl. Phys. Lett.* **1991**, *59*, 3162.
(11) Mokler, S. M.; Ohtani, N.; Xie, M. H.; Zhang, J.; Joyce, B. A. *Appl. Phys. Lett.* **1992**, *61*, 2548.
(12) Malik, R.; Gulari, E.; Li, S. H.; Bhattacharya, P. K. *J. Appl. Phys.* **1993**, *73*, 5193.
(13) Russell, N. M.; Breil and, W. G. *J. Appl. Phys.* **1993**, *73*, 3525.
(14) Lee, I. M.; Wang, W. C.; Neudeck, G. W.; Takoudis, C. G. *Chem. Eng. Sci.* **1996**, *51*, 2681.
(15) Hirose, F.; Sakamoto, H. *Microelectron. Eng.* **1998**, *43*−*44*, 635.
(16) Kim, H.; Taylor, N.; Bramblett, T. R.; Greene, J. E. *J. Appl. Phys.* **1998**, *84*, 6372.
(17) Ning, B. M. H.; Crowell, J. E. *Surf. Sci.* **1993**, *295*, 79.
(18) Wu, Y. M.; Baker, J.; Hamilton, P.; Nix, R. M. *Surf. Sci.* **1993**, *295*, 133.
(19) Wu, Y. M.; Nix, R. M. *Surf. Sci.* **1994**, *306*, 59.
(20) Russell, N. M.; Ekerdt, J. G. *Surf. Sci.* **1996**, *369*, 51.
(21) Angot, T.; Louis, P. *Phys. Rev. B* **1999**, *60*, 5938.
(22) Ku, J. H.; Nemanich, R. J. *J. Appl. Phys.* **1996**, *80*, 4715.
(23) Kim, H.; Taylor, N.; Abelson, J. R.; Greene, J. E. *J. Appl. Phys.* **1997**, *82*, 6062.
(24) Kim, H.; Desjardins, P.; Abelson, J. R.; Greene, J. E. *Phys. Rev. B* **1998**, *58*, 4803.
(25) Duke, C. B. *Chem. Rev.* **1996**, *96*, 1237.
(26) Grant, M. W.; Dieleman, D. J.; Boshart, M. A.; Seiberling, L. E. *Phys. Rev. B* **1994**, *49*, 16534.
(27) Fontes, E.; Patel, J. R.; Comin, F. *Phys. Rev. Lett.* **1994**, *72*, 1131.
(28) Patthey, L.; Bullock, E. L.; Abukawa, T.; Kono, S.; Johansson, L. S. O. *Phys. Rev. Lett.* **1995**, *75*, 2538.
(29) Oyanagi, H.; Sakamoto, K.; Shioda, R. *J. Phys. IV* **1997**, *7*, 669.
(30) Sumitomo, K.; Nishioka, T.; Ogino, T. *J. Vac. Sci. Technol. A* **1997**, *15*, 1537.
(31) Chen, X.; Saldin, D. K.; Bullock, E. L.; Patthey, L.; Johansson, L. S. O.; Tani, J.; Abukawa, T.; Kono, S. *Phys. Rev. B* **1997**, *55*, R7319.
(32) Kobayashi, Y.; Isaka, H.; Ogino, T. *Appl. Surf. Sci.* **1998**, *132*, 314.
(33) Iwawaki, F.; Tomitori, M.; Nishikawa, O. *Surf. Sci.* **1992**, *266*, 285.
(34) Jones, D. E.; Pelz, J. P.; Xie, Y. H.; Silverman, P. J.; Fitzgerald, E. A. *Surf. Sci.* **1995**, *341*, L1005.
(35) Tomitori, M.; Watanabe, K.; Kobayashi, M.; Nishikawa, O. *J. Vac. Sci. Technol. B* **1994**, *12*, 2022.
(36) Liu, F.; Wu, F.; Lagally, M. G. *Chem. Rev.* **1997**, *97*, 1045.
(37) Guo, L. W.; Huang, Q.; Li, Y. K.; Ma, S. L.; Peng, C. S.; Zhou, J. M. *Surf. Sci.* **1998**, *406*, L592.
(38) Sinniah, K.; Sherman, M. G.; Lewis, L. B.; Weinberg, W. H.; Yates, J. T.; Janda, K. C. *J. Chem. Phys.* **1990**, *92*, 5700.
(39) Kolasinski, K. W. *Int. J. Mod. Phys. B* **1995**, *9*, 2753.
(40) Doren, D. J. *Adv. Chem. Phys.* **1996**, *95*, 1.
(41) Boland, J. J. *Phys. Rev. Lett.* **1991**, *67*, 1539.
(42) D'Evelyn, M. P.; Yang, Y. M. L.; Sutcu, L. F. *J. Chem. Phys.* **1992**, *96*, 852.
(43) Kolasinski, K. W.; Shane, S. F.; Zare, R. N. *J. Chem. Phys.* **1992**, *96*, 3994.
(44) Flowers, M. C.; Jonathan, N. B. H.; Liu, Y.; Morris, A. *J. Chem. Phys.* **1993**, *99*, 7038.
(45) Jing, Z.; Whitten, J. L. *J. Chem. Phys.* **1993**, *98*, 7466.
(46) Jing, Z.; Lucovsky, G.; Whitten, J. L. *Surf. Sci.* **1993**, *296*, L33.
(47) Wu, C. J.; Ionova, I. V.; Carter, E. A. *Surf. Sci.* **1993**, *295*, 64.
(48) Nachtigall, P.; Jordan, K. D.; Sosa, C. *J. Chem. Phys.* **1994**, *101*, 8073.
(49) Pal, S.; Doren, D. *J. Chem. Phys.* **1995**, *103*, 1232.
(50) Pehlke, E.; Scheffler, M. *Phys. Rev. Lett.* **1995**, *74*, 952.
(51) Radeke, M. R.; Carter, E. A. *Phys. Rev. B* **1996**, *54*, 11803.
(52) Radeke, M. R.; Carter, E. A. *Surf. Sci.* **1996**, *355*, L289.
(53) Brenig, W.; Gross, A.; Hofer, U.; Russ, R. *Phys. Status Solidi A*−*Appl. Res.* **1997**, *159*, 75.
(54) Kratzer, P.; Pehlke, E.; Scheffler, M.; Raschke, M. B.; Hofer, U. *Phys. Rev. Lett.* **1998**, *81*, 5596.
(55) Biedermann, A.; Knoesel, E.; Hu, Z.; Heinz, T. F. *Phys. Rev. Lett.* **1999**, *83*, 1810.
(56) Lin, D. S.; Chen, R. P. *Phys. Rev. B* **1999**, *60*, R8461.
(57) Penev, E.; Kratzer, P.; Scheffler, M. *J. Chem. Phys.* **1999**, *110*, 3986.
(58) Buehler, E. J.; Boland, J. J. *Science* **2000**, *290*, 506.
(59) Zimmermann, F. M.; Pan, X. *Phys. Rev. Lett.* **2000**, *85*, 618.
(60) Durr, M.; Raschke, M. B.; Pehlke, E.; Hofer, U. *Phys. Rev. Lett.* **2001**, *86*, 123.
(61) Steckel, J. A.; Phung, T.; Jordan, K. D.; Nachtigall, P. *J. Phys. Chem. B* **2001**, *105*, 4031.
(62) Hofer, U.; Li, L. P.; Heinz, T. F. *Phys. Rev. B* **1992**, *45*, 9485.
(63) D'Evelyn, M. P.; Cohen, S. M.; Rouchouze, E.; Yang, Y. L. *J. Chem. Phys.* **1993**, *98*, 3560.
(64) Mui, C.; Bent, S. F.; Musgrave, C. B. *J. Phys. Chem. B*, submitted.
(65) Mui, C.; Bent, S. F.; Musgrave, C. B. *J. Phys. Chem. A* **2000**, *104*, 2457.
(66) Hohenberg, P.; Kohn, W. *Phys. Rev.* **1964**, *136*, B864.
(67) Kohn, W.; Sham, L. J. *Phys. Rev.* **1965**, *140*, A1133.
(68) Becke, A. D. *J. Chem. Phys.* **1993**, *98*, 5648.
(69) Frisch, M. J.; Trucks, G. W.; Schlegel, H. B.; Scuseria, G. E.; Robb, M. A.; Cheeseman, J. R.; Zakrzewski, V. G.; Montgomery, J. A., Jr.; Stratmann, R. E.; Burant, J. C.; Dapprich, S.; Millam, J. M.; Daniels, A. D.; Kudin, K. N.; Strain, M. C.; Farkas, O.; Tomasi, J.; Barone, V.; Cossi, M.; Cammi, R.; Mennucci, B.; Pomelli, C.; Adamo, C.; Clifford, S.; Ochterski, J.; Petersson, G. A.; Ayala, P. Y.; Cui, Q.; Morokuma, K.; Malick, D. K.; Rabuck, A. D.; Raghavachari, K.; Foresman, J. B.; Cioslowski, J.; Ortiz, J. V.; Stefanov, B. B.; Liu, G.; Liashenko, A.; Piskorz, P.; Komaromi, I.; Gomperts, R.; Martin, R. L.; Fox, D. J.; Keith, T.; Al-Laham, M. A.; Peng, C. Y.; Nanayakkara, A.; Gonzalez, C.; Challacombe, M.; Gill, P. M. W.; Johnson, B.; Chen, W.; Wong, M. W.; andres, J. L.; Gonzalez, C.; Head-Gordon, M.; Replogle, E. S.; Pople, J. A. *Gaussian 98*, revision A.5; Gaussian, Inc.: Pittsburgh, PA, 1998.
(70) Hierlemann, M.; Werner, C.; Spitzer, A. *J. Vac. Sci. Technol. B* **1997**, *15*, 935.
(71) Kang, J. K.; Musgrave, C. B. *Phys. Rev. B* **2001**, *64*, 5330.
(72) Widjaja, Y.; Musgrave, C. B. *Surf. Sci.* **2000**, *469*, 9.